약학박사학위논문

염증성 암세포에서의 caspase-8에 의존적인 lysyl-tRNA synthetase의 exosome을 통한 분비 기전 연구

Caspase-8-dependent exosomic secretion of lysyl-tRNA synthetase from inflammatory cancer

2017 년 8월

서울대학교 융합과학기술대학원
분자의학 및 바이오제약학과 세포유전체전공
김 상 범

염증성 암세포에서의 caspase-8에 의존적인 lysyl tRNA synthetase의 exosome을 통한 분비 기전 연구

Caspase-8-dependent exosomic secretion of lysyl-tRNA synthetase from inflammatory cancer

지도교수 김 성 훈

이 논문을 약학박사학위논문으로 제출함
2017 년 8월

서울대학교 융합과학기술대학원
분자의학 및 바이오제약학과 세포유전체전공
김상범

김상범의 박사학위논문을 인준함
2017 년 8월

위 원 장	강 창 율	(인)
부 위 원 장	김 성 훈	(인)
위 원	이 정 원	(인)
위 원	김 필 한	(인)
위 원	전 영 호	(인)

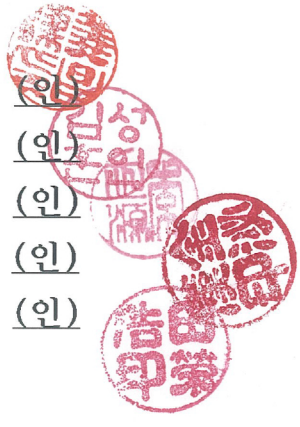

Contents

Abbreviations used

ARS, aminoacyl-tRNA synthetase; BFA, brefeldin A; BiFC, bimolecular fluorescence complementation; ILV, intraluminal vesicle; KRS, lysyl-tRNA synthetase; LPS, lipopolysaccharide; MITF, microphthalmia associated transcription factor; MSC, multi-tRNA synthetase complex; MVB, multivesicular body; WT, wild-type.

List of Figures

Abstract

Although lysyl-tRNA synthetase (KRS), an enzyme for protein synthesis, is secreted from cancer cells to trigger inflammatory responses, its secretion mechanism is not understood. Here we show that KRS is secreted via exosomes from cancer cells. KRS is located within the lumen of exosomes and released from the exosomes that are ruptured near the target cells. The N-terminal 12 amino acid of KRS was cleaved by caspase-8 upon starvation. The N-terminal cleavage exposed the PDZ-binding motif located in its C-terminal end. Syntenin bound to the exposed PDZ-binding motif of KRS and facilitated the dissociation of KRS from multi-tRNA synthetase complex for exosomic secretion. The isolated KRS-containing exosomes induced migration and TNF-α secretion of macrophages and KRS showed significant contribution to these activities. These results suggest exosomes as a secretion vehicle for KRS and its functional connection with caspase-8-mediated inflammation provoked by cancer cells.

Keywords : exosome, lysyl-trna synthetase, syntenin, caspase-8, inflammation

Student number : 2010-31385

Introduction

Aminoacyl-tRNA syntetases (ARSs) are known as essential enzymes for protein synthesis, charging amino acids to their cognate tRNAs (Ibba and Soll, 2000). However, they are now newly recognized as multi-faceted signal mediators, dynamically connected to diverse signal pathways (Guo and Schimmel, 2013). Among them, many activities involve the secretion of ARSs into extracellular space (Son et al., 2014). The secreted ARSs have been reported to play roles in the control of angiogenesis (Mirando et al., 2014), immune responses (Han et al., 2007; Nechushtan et al., 2009; Park et al., 2005b)), tissue regeneration (Park et al., 2005c) and tumorigenesis (Choi et al., 2011; Park et al., 2005a; Park et al., 2012). However, it remains unanswered how they are secreted. Among the secreted ARSs, KRS was previously shown to be secreted from cancer cells to induce inflammatory responses. To have an insight into secretion mechanism of ARSs, here we focused on the secretion of KRS and investigated in-depth how it is secreted from cancer cells.

Exosomes are small extracellular vesicles originating from the

endosome. Exosomes have established characteristics of 1.15-1.19g/ml density, 50-150nm diameter, and cup-shape electronic microscopic morphology (Bobrie and Thery, 2013). These exosomes have diverse component - membrane protein, receptor, kinase, other cytosol protein, microRNA, mRNA, tRNA, lipids and several other functions. It is an important intracellular communication method. Exosomes transfer cargo protein to recipient cells and contribute to immunological processes in tumor progression and metastasis (Raposo and Stoorvogel, 2013). These exosomes are generated from the endosome that are produced by plasma membrane budding. Inward budding makes multi-vesicular bodies (MVBs) and intraluminal vesicles (ILVs). The formation of ILVs requires the endosomal sorting complex for transport (ESCRT) machinery and these machinery indicates ubiquitination of membrane protein, thereby inducing intraluminal vesicles (Robbins and Morelli, 2014). Ceramide and other lipids also induce exosome biogenesis through ESCRT independent mechanism. Recently, a new mechanism of exosome biogenesis was mentioned that syntenin controls the formation of exosome ubiquitination independent manner (Baietti et al., 2012). The specific

mechanism syntenin dependent exosome pathway is induced so that the syntenin-syndecan complex interacts with ALIX through its N-terminal LYPXnL motif. Since ALIX is an auxiliary component of ESCRT, this interaction induces ESCRT machinery binding to syntenin complex and produces ILV which has syndecan cargo protein, like FGFR1, in MVB. In this sequential mechanism, syndecan cleavaged by heparanse induces intraluminal budding of syndecan-syntenin-alix and syndecan cargo protein complex in endosomes (Roucourt et al., 2015). In previous report, we already notice that PDZ domain of syntenin could interact with KRS (Meerschaert et al., 2008). However, the function of KRS-syntenin complex was not clear yet.

Caspase family is well known protease proteins in apoptosis and inflammation. This protease family is classified into two sub-families; one is regulator of inflammation (caspases-1, -4, -5, -12). and the other is regulator of apoptosis (caspases-3, -6, -7, -8, -9)(Van Damme et al., 2005; McIlwain et al., 2015). Among these, caspase-1 is the major protein that induces inflammation. Upon bacteria infection, caspase-1 is activated and build inflammasome with

different types of scaffolding proteins. These scaffolding proteins are assembly of different inflammasomes depending on various specific pathogen- or danger associated molecular patterns (PAMPs and DAMPs). Assembled caspase-1 inflammasome cleaves pro-IL-1β, pro-IL-18, pro-IL-33 to activate IL-1β, IL-18, IL-33. Canonical role of caspase8 is initiating the apoptosis process. Fas ligand binds to Fas receptor and induces pro caspase-8 cleavage. Caspase-8 truncates pro-caspase-3 to caspase-3 and induces cell apoptosis. Beside classical role of caspase 8 in apoptosis, its role in pro il 1b activation was recently studied from other group. recently studies showed that caspase-8 induced pro-IL-1β activation. Two hypothetical mechanisms were mentioned; one is the caspase-8 inflammasome dependent, another is caspase-8 inflammasome independent pathway. Caspase-8 inflammasome dependent pathway starts with either fungi or mycobacterium binding to dectin-1 and phosphorylates Syk kinase (McIlwain et al., 2015; Gringhuis et al., 2012). Through PKCδ activation, caspase-8 inflammasome is assembled with CARD9, Bcl-10, MALT1, ASC. Activated caspase-8 inflammasome cleaves pro- IL-1β to IL-1β. IL-1β secretion is dramatically reduced in

caspase-8 -/-, Ripk3-/- dendritic cells compared with Ripk3-/- or WT dendritic cell (Antonopoulos et al., 2013). Caspase-8 inflammasome independent pathway induces apoptotic signaling like CD95L, and ER stress. In this signaling pathway, IL-1β secretion is independent of caspase-8 inflammation components such as NLRP3, NRC4, and ASC. This evidence mean caspase-8 can induce inflammation and can regulate apoptosis and inflammation in immune cell. Because caspase-8 is well-known apoptosis caspase, loss of caspase-8 expression can help the cancer progression. Even some cancer types are upregulated with caspase-8 expression level but its reason is not yet unveiled.

Human cytosolic KRS is comprised of 574 amino acid (aa) in which the anticodon-binding (S70-P214) and catalytic domains (L220-K574) are embedded (Guo et al., 2008), (Fig. 1a). It also contains a unique N-terminal extension (Guo et al., 2010). Human KRS can undergo dynamic structural transformation guided by specific phosphorylation to exert distinct roles. For instance, it is phosphorylated at S207 in the activated mast cells (Ofir-Birin et al., 2013; Yannay-Cohen et al., 2009). S207 is located at the

junction of the two functional domains and its phosphorylation pushes the two domains apart so that it does not work as the enzyme for tRNA charging anymore. The resulting S207 phosphorylated KRS is then translocated into nucleus for transcriptional control via MITF. Upon laminin treatment, KRS is phosphorylated at T52 that is located in the N-terminal extension that is unique for higher eukaryotic KRS. This phosphorylation induces unfolding of the N-terminal extension that is then guided to plasma membrane. The membrane-bound KRS can interact with 67kDa laminin receptor to promote cell migration (Kim et al., 2012) and this function is also implicated in cancer metastasis (Kim et al., 2014). In this work, we investigated how KRS is secreted to extracellular space and whether any post-translational modification would be involved in this process.

Results

KRS secretion via exosomes

Since many proteins are secreted via ER-golgi pathway (Lacy and Stow, 2011), we investigated whether the secretion of KRS would also involve this pathway using Brefeldin A (BFA) that is the inhibitor of the ER-Golgi secretion pathway (Rosa et al., 1992). Following the previous report, we induced KRS secretion by subjecting HCT116 cells to starvation (with and without TNF-α) and checked how the BFA treatment would affect the secretion and found that BFA did not affect KRS secretion (Fig 1B). Besides, we examined the potential signal peptide in the N-terminal region of KRS for the secretion through ER-Golgi pathway using SignalP database (http://www.cbs.dtu.dk/services/signalP/) and found no clue to the presence of signal peptide (data not shown). Instead, KRS contains the PDZ domain-binding motif in its C-terminal end (Fabre et al., 2000) (Fig. 1A) which can be used for the interaction with syntenin that is known to be involved in exosome secretion (Baietti et al., 2012; Meerschaert et al., 2008). Based on these results, we

assumed that KRS may secrete via extracellular vesicles such as exosomes.

To see whether the KRS secretion would involve secretory vesicles, we subjected the complete and starvation culture media of HCT116 cells to centrifugation at 100,000 g and obtained the pellet. We then lysed the proteins from the isolated vesicles in the pellets and checked the presence of KRS by immunoblotting with anti-KRS antibody. Higher amount of KRS was detected in the vesicles isolated from the starvation medium (Fig. 1C). We examined the condition that can induce the secretion of KRS from HCT116 cells. Among all the tested conditions (Starvation, Inflammation by TNF-α, Reactive Oxygen Stress (ROS) by Sodium Arsenite (Barchowsky et al., 1999; Ruiz-Ramos et al., 2009), Hypoxia by $CoCl_2$(Piret et al., 2002) and ER stress by Tunicamycin), KRS secretion was most prominent upon starvation (Fig. 1D). Interestingly, the size of KRS in the vesicle appeared to be smaller than that of the cytosolic KRS, suggesting a potential peptide cleavage of KRS during the secretion process (see below). Density-gradient centrifugation analyses of the isolated

vesicles showed that KRS is harbored in the fractions with the density range of 1.09 - 1.15 g/ml that also contained syntenin, a factor crucial for exosome secretion (Baietti et al., 2012; Thery et al., 2009) (Fig. 1E). Opti-prep gradient centrifugation suggested that the KRS-containing vesicles would have an average of 147.3 nm in diameter (Fig. 1F). We subjected the isolated vesicles to electron microscopic analysis and found that they would have a typical cup shape (Fig. 1G) that are morphologically similar to typical exosomes (Thery et al., 2009).

We also investigated whether KRS secretion was affected by suppression of Rab GTPases (Rab11a, Rab27a, Rab35) which have been suggested to play a role in exosome shedding (Hsu et al., 2010; Ostrowski et al., 2010; Savina et al., 2005). The KRS secretion was differentially reduced by the suppression of Rab proteins (Fig. 2A), implying that KRS-exosomes might be exported out of cells in a Rab-dependent manner. Since ESCRT-III proteins were previoulsy suggested to induce luminal vesicle formation of MVB and exosomic secretion of syntenin (Baietti et al., 2012), we also examined whether

KRS secretion would be affected by the suppression of ESCRT-III proteins and observed the reduction of KRS and syntenin secretion by the suppression of each ESCRT-III component (CHMP1a, 2a, 3, 4a, 4b, 6 and 7) (Fig. 2B). These results further support the syntenin-dependent exosomal secretion pathway.

We then determined the location of KRS in the isolated exosomes by electron microscopy with immunogold staining of KRS and CD63, the typical membrane marker of exosome (Marzesco et al., 2005; Thery et al., 2002), with their specific antibodies. While CD63 was located in the membrane of the isolated exosomes, KRS was mostly located in the lumen (Fig. 3A, 3B). We further determined the KRS topology in the isolated exosomes by trypsin treatment, and observed that KRS and syntenin were resistant whereas CD63 was sensitive to trypsin digest (Fig. 3C). These results further suggest that KRS is localized within the lumen of isolated exosomes.

The naked KRS was previously shown to activate macrophages. To determine whether KRS in the lumen of exosomes can activate macrophages, we treated macrophages with KRS-containing exosomes

and followed the movement of KRS from exosomes to macrophages by immunogold-staining electron microscopy. KRS located in the lumen of exosomes (Fig. 3D) was released by the rupture of the exosomes (Fig. 3E) and introduced into macrophages (Fig. 3F).

To further confirm this observation, we expressed C-terminally Myc-tagged KRS (KRS-Myc) in HCT116 cells and prepared exosomes harboring KRS-Myc. We then treated macrophages with these exosomes and monitored whether KRS-Myc was sensitive to proteolytic cleavage. If KRS-Myc would be taken up to macrophages as naked protein, it would be sensitive to proteolytic cleavage. We did not detect intact KRS-Myc in macrophages that were assayed at different time intervals, (Fig. 3G), further supporting the electron microscopic observation.

To determine whether KRS is specifically recruited to the starvation-induced exosomes, we examined the presence of nine different ARSs and found only KRS in the isolated exosomes (Fig. 4A), suggesting the preferential recruitment of KRS to starvation-induced exosomes. We also tested several different cancer

cell lines for the secretion of KRS- exosomes and found that MCF7 cells also secreted KRS (Fig. 4B).

Requirement of syntenin for KRS secretion

A potential interaction of KRS was previously suggested with syntenin that plays a crucial role in exosome biogenesis and secretion (Baietti et al., 2012; Meerschaert et al., 2008). We thus investigated whether syntenin would indeed play a role in the secretion of KRS. First, we performed co-immunoprecipitation assay of syntenin and KRS in the complete, starved and TNF-α treatment conditions. The starvation condition (with and without TNF-α) increased the interaction of the two proteins compared to that of the complete medium (Fig. 5A). The cellular interaction of the two proteins was also monitored by BiFC (Bimolecular Fluorescence Complementation) assay using green fluorescence Venus protein. The 173aa N- and 155aa C-terminal fragments of Venus were fused to the C-terminal ends of KRS and syntenin, respectively. The interaction of the two proteins would restore Venus green fluorescence while either alone

would not. We incubated HCT116 cells expressing the two fusion proteins, KRS-VN173 and syntenin-VC155 in the complete and starvation media and the generation of green fluorescence was measured. The fluorescence was only observed in the starvation condition (Fig. 5B). To see whether syntenin is required for KRS secretion, we suppressed the cellular levels of syntenin with its specific siRNA and checked the effect on the KRS secretion. The amount of secreted KRS was decreased when syntenin was suppressed with its siRNA in dose-dependent manner (Fig. 5C). The syntenin knockdown also decreased the amount of KRS as well as syntenin itself in the isolated exosomes (Fig. 5D).

To see whether the C-terminal PDZ-binding motif of KRS is critical for the syntenin binding and exosomic secretion of KRS, we first compared the interaction of KRS WT and the C-terminal 5aa deleted mutant (△C5) with syntenin by co-immunoprecipitation and found that KRS △C5 mutant showed the reduced ability to bind to syntenin (Fig. 5E). We then examined whether KRS WT and △C5 mutant would show difference in secretion and found that the deletion

of PDZ-binding motif reduced the secretion and exosome incorporation ability of KRS (Fig. 5F and G, respectively). To further validate the importance of the PDZ-binding motif, we introduced alanine substitutions to the four C-terminal residues (C4A mutant) (Manes et al., 2010; Wieman et al., 2009), and monitored how these mutations affected recruitment of KRS into exosomes. The amount of KRS C4A mutant was significantly lower than that of KRS WT in the isolated exosomes (Fig. 5H). All of these results suggest that syntenin binding to the C-terminal PDZ-binding motif facilitates exosomic secretion of KRS.

The role of the KRS N-terminus in secretion

We found that KRS isolated from the isolated exosomes moved faster in gel electrophoresis than cytosolic KRS, suggesting that a portion of KRS might be cleaved off during the secretion process (Fig. 6A). To determine the cleavage site, we expressed KRS with Myc tag fused at the N- or C-terminal end in HCT116 cells and subjected KRS in the secreted exosomes to immunoblot analysis with anti-Myc

antibody. While we detected KRS-Myc (fused to the C-terminal) but not Myc-KRS (fused to the N-terminal) (Fig. 6B), implying that the N-terminal end would be truncated. We also prepared the double-tagged form of KRS in which Strep and Myc tags were fused to the N- and C-terminal ends, respectively, and expressed it in HCT116 cells. The secreted KRS was detected with anti-Myc but not with anti-Strep antibody (Fig. 6C), further supporting the N-terminal cleavage of KRS for secretion. Next, we attached the N- and C-terminal domains of Renilla luciferase (Kerppola, 2008; Ofir-Birin et al., 2013) to the N- and C-terminal ends of KRS, respectively, and used this fusion protein to monitor the secretion-induced KRS cleavage. While the intact KRS would bring the two domains of Renilla luciferase into proximity to recover the luciferase activity, the cleavage of KRS would ablate the Binary Fluorescence Complementation (BiFC) of the two Renilla luciferase domains. Indeed, as HCT116 cells were starved, the BiFC signal was decreased in time-dependent manner (Fig. 6D). We then expressed the GFP-KRS fusion protein in HCT116 cells and incubated the cells in the starvation condition. The cytosolic emergence of GFP resulting from

the cleavage of GFP-KRS showed the similar kinetic pattern to that of KRS secretion (Fig. 6E). All of these results indicate that KRS is cleaved at its N-terminal region for secretion.

We next determined the exact cleavage location in KRS. We first prepared a series of the N-terminal deletion mutants of Myc-KRS and compared the effects of the deletion on KRS secretion. Among the tested mutants, the secretion of KRS mutants, △N20, △N30 and △N40 (the N-terminal 20, 30 and 40aa deleted, respectively) was observed, but not KRS WT and mutant △N10 (Fig. 7A), suggesting that the N-terminal cleavage would occur somewhere from the 11^{th} to 20^{th} residue. We further prepared the Myc-KRS mutants, △N11 and △N12 and conducted the same experiments above, and found that Myc-KRS △N12, but not △N10 and △N11, was detected (Fig. 7B). Combined together, the results suggest that the secretion-induced cleavage should occur between at the 12^{th} residue. To further confirm this, we mutated aspartic acid residue at the position of 12 to alanine (D12A) and checked whether this mutation would affect the secretion of KRS. KRS-Myc D12A

mutant was not detected in the culture medium, indicating that the mutation deprived the ability of secretion (Fig. 7C). We also monitored the secretion-induced cleavage of this mutant using BiFC Renilla luciferase as above. The Renilla luciferase activity was reduced by starvation in KRS WT, but not in the D12A mutant (Fig. 7D). Likewise, the starvation-induced cleavage of GFP-KRS was also not observed in GFP-KRS D12A mutant in contrast to GFP-KRS WT (Fig. 7E). When we subjected Myc-KRS WT and△N12 mutant isolated from the secreted exosomes to immunoblotting with anti-Myc antibody and found only Myc-KRS △N12, but not WT, further indicating that the cleavage would occur at D12 position (Fig. 7F). Comparison of KRS-Myc WT and D12A mutant for exosome incorporation, only KRS WT was detected in the isolated exosomes, further confirming the importance of D12 cleavage for the exosome incorporation and secretion of KRS (Fig. 7G).

The role of caspase-8-mediated N-terminal cleavage in syntenin interaction

We next determined the enzyme responsible for the cleavage of the N-terminal 12aa of KRS for its secretion. Interestingly, the N-terminal peptide of KRS contains the consensus caspase (V-X-X-D especially for 3, 6 and 8) substrate sequence (Van Damme et al., 2005) (Fig. 1A). To determine whether any of the known caspases is required for the N-terminal truncation and secretion of KRS, we treated HCT116 cells with Pan-caspase inhibitor and checked its effect on KRS secretion and KRS truncation. The starvation-induced KRS secretion and truncation were significantly inhibited by the treatment of Pan-caspase inhibitor (Fig. 8A, 8B), suggesting the involvement of caspase activity for the secretion. To determine the caspase that is responsible for the KRS cleavage, we suppressed one of caspases-3, -6, -8 and -9 with their specific siRNAs and specific caspase inhibitor compared their effects on the secretion of KRS. Among them, the knockdown and inhibitor of caspase-8 specifically blocked the KRS secretion (Fig. 8C, 8D). We also observed the KRS level in the exosomes was reduced when HCT116 cells were treated with caspase-8 inhibitor (Z-VAD-IETD) (Fig. 8E). The effect of caspase 8 inhibitor on the KRS cleavage was

also monitored using BiFC Renilla luciferase-fused KRS and GFP-KRS truncation. The Renilla luciferase activity was reduced by starvation, but recovered by the treatment of caspase-8 inhibitor (Fig. 8F). And also GFP-KRS truncation was increased by starvation, but recovered by the treatment of caspase-8 inhibitor (Fig. 8G). We next examined whether the expression level of caspase-8 is affected by starvation, and found that caspase-8 level is specifically increased upon starvation in time-dependent manner while the levels of other caspases did not (Fig. 8H). We also found that the exogenously introduced caspase-8 increased the levels of secreted KRS in dose-dependent manner (Fig. 8I). Then, we investigated whether inhibition of caspase-8 would affect the interaction of KRS with syntenin by co-immunoprecipitation and found that the starvation-induced interaction of the two proteins was inhibited by the treatment of caspase-8 inhibitor (Fig. 9A), suggesting the importance of the caspase-8 cleavage of the KRS N-terminal peptide for the interaction of KRS with syntenin. We also compared the interaction of KRS WT and D12A mutant with syntenin by co-immunoprecipitation in starvation condition and found that the

D12A mutant showed reduced interaction with syntenin (Fig. 9B). The starvation-induced interaction of the two proteins was also observed by BiFC as above and the effects of D12A mutation and caspase 8 inhibition on the interaction was examined. In contrast to the pair of KRS WT and syntenin, KRS D12A mutation or Z-VAD-IETD treatment inhibited the generation of green fluorescence (Fig. 9C). Combined together, caspase-8 was identified as the enzyme responsible for the cleavage at D12 of KRS that facilitates its interaction with syntenin and secretion.

Syntenin-dependent dissociation of KRS from multi-tRNA synthetase complex

A majority of KRS would exist as a component of the multi-tRNA synthetase complex (MSC) in cytosol. We thus investigated whether the secretion of KRS would require its dissociation from MSC using gel filtration chromatography. When proteins extracted from HCT116 cells (complete and starvation condition) were subjected to gel filtration, starvation-induced dissociation of KRS from MSC was

increased, but not of EPRS, another component of MSC that is known to be dissociated from MSC by IFN-γ (Sampath et al., 2004) (Fig. 10A). We then examined whether the N12aa truncation would affect the dissociation of KRS from MSC. We starved HCT116 cells in the absence and presence of caspase-8 inhibitor and cellular MSC was immunoprecipitated with anti-EPRS antibody. The portion of KRS not bound to MSC was detected by immunoblotting of KRS remained in the immune-depleted supernatants after removing the immunoprecipitates. The KRS present in the immune-depleted fraction was decreased by the treatment of caspase-8 inhibitor (Fig. 10B), suggesting that caspase-8-mediated N-terminal cleavage of KRS can enhance the dissociation of KRS from MSC. Using the same method, we examined whether the DN12 or cleavage-defective D12A mutation and syntenin would affect the dissociation of KRS from MSC. In contrast to KRS WT and DN12 mutant, KRS D12A mutant was not detected in the immune-depleted supernatants (Fig. 10C). Also, knockdown of syntenin reduced the amount of KRS in the immune-depleted fractions. We also compared the starvation-induced dissociation of KRS WT and △C5 mutant from MSC as above, and

found that the △C5 mutant level was significantly reduced in the immune-depleted fraction (Fig. 10D). All these results suggest that the caspase 8-mediated N-terminal cleavage of KRS and the interaction of the resulting KRS with syntenin would facilitate the dissociation of KRS from MSC.

Knowing that syntenin would facilitate the dissociation of KRS from MSC and its extracellular secretion through exosome, we further investigated whether syntenin can guide KRS to Alix, the known marker for multivesicular body (MVB) (Baietti et al., 2012; Matsuo et al., 2004; Odorizzi, 2006), from which exosomes are secreted. For this, we visualized the KRS-syntenin complex using BiFC method as above and tested whether the BiFC green fluorescence signals (resulting from the complex formation between KRS and syntenin) are co-localized with Alix that was labeled with mCherry (red fluorescence). The KRS-syntenin complex (green fluorescence) was generated upon starvation as shown before and it was co-localized with the fraction of mCherry-Alix (Fig. 10E), suggesting that syntenin can guide the N-terminal cleaved KRS from

MSC to MVB. Since Alix is known to generate intraluminal vesicles (ILV) in MVB with the client proteins from endosome, we checked again whether KRS is located in the vesicles harbored within MVB using immunogold-staining EM with anti-KRS antibody as above. The KRS-specific immunogold particles were enriched in the vesicles located within MVB of the HC116 cells under starvation (Fig. 10F), suggesting that KRS-containing vesicles are formed within MVB.

Inflammatory activity of KRS-harboring exosomes

KRS secreted from cancer cells was previously shown to trigger inflammatory responses when it was treated to macrophages (Park et al., 2005b). Here we observed that KRS can be released from the exosomes and introduced macrophages (Fig. 3D-F), suggesting that these exosomes would exert the extracellular activities shown by the naked KRS. We thus compared the naked KRS WT, DN12 mutant protein and KRS-containing exosomes in their ability to induce various cytokines and factors that are the known markers for M1- and M2-type macrophages, and found that they all showed the

similar activities, inducing TNF-α, CRG-2, IL6 and MMP9 from RAW 264.7 cells (Fig. 11A, 11B) that are the signatures for M1-type macrophages (Mantovani et al., 2002) with EC50 values of 83.4 nM (KRS WT protein), 70.7 nM (KRS △N12 mutant) and 2.89 mg/ml (KRS-exosome) (Fig. 11C). They also induced macrophage migration (Fig. 11D). These results suggest that the truncation of the N-terminal 12aa did not ablate the immune stimulatory activity of KRS WT and KRS-containing exosomes would be functionally equivalent to the naked KRS in inducing M1 polarization of macrophages. To evaluate the functional significance of KRS in the isolated exosomes, we compared the abilities of the isolated exosomes from the si-control and si-KRS-treated HCT116 cells to induce TNF-α. Knockdown of KRS with its specific si-KRS significantly reduced the content of KRS in exosomes while not affecting those of other components such as syntenin and Alix (Fig. 12A). The exosomes obtained from the si-KRS-treated cells showed reduced TNF-α-inducing and macrophage migration activities compared to those of si-control-treated cells (Fig. 12B, 12C). To confirm these data in vivo, we monitored the effect of the isolated exosomes from

the si-KRS and si-control cells on the migration of macrophages and neutrophils in vivo by intravital confocal microscopy using GFP-LysM mice in which the mobility of macrophages and monocytes can be monitored by green fluorescence (Choe et al., 2013; Faust et al., 2000). When we first injected the naked KRS (labeled as red fluorescence) in vivo, we observed that the injected KRS attracted significantly enhanced immune cells compared with BSA (Fig. 12D-E). Similarly, the exosomes isolated from the si-control and si-KRS-treated HCT116 cells were labeled with red fluorescence DiI and injected into GFP-LysM mice. The si-control exosomes induced infiltration of macrophages and monocytes more strongly compared to si-KRS exosomes and BSA (Fig. 12F-G). Using the same method, we further compared the immune cell attracting effects of the cells expressing EV, KRS WT and D12A mutant. After confirming that KRS D12A mutant showed the reduced capability of secretion (Fig. 12H), we observed that the cells expressing this mutant showed the reduced immune cell attracting capability compared to those expressing KRS WT (Fig. 12I-J).

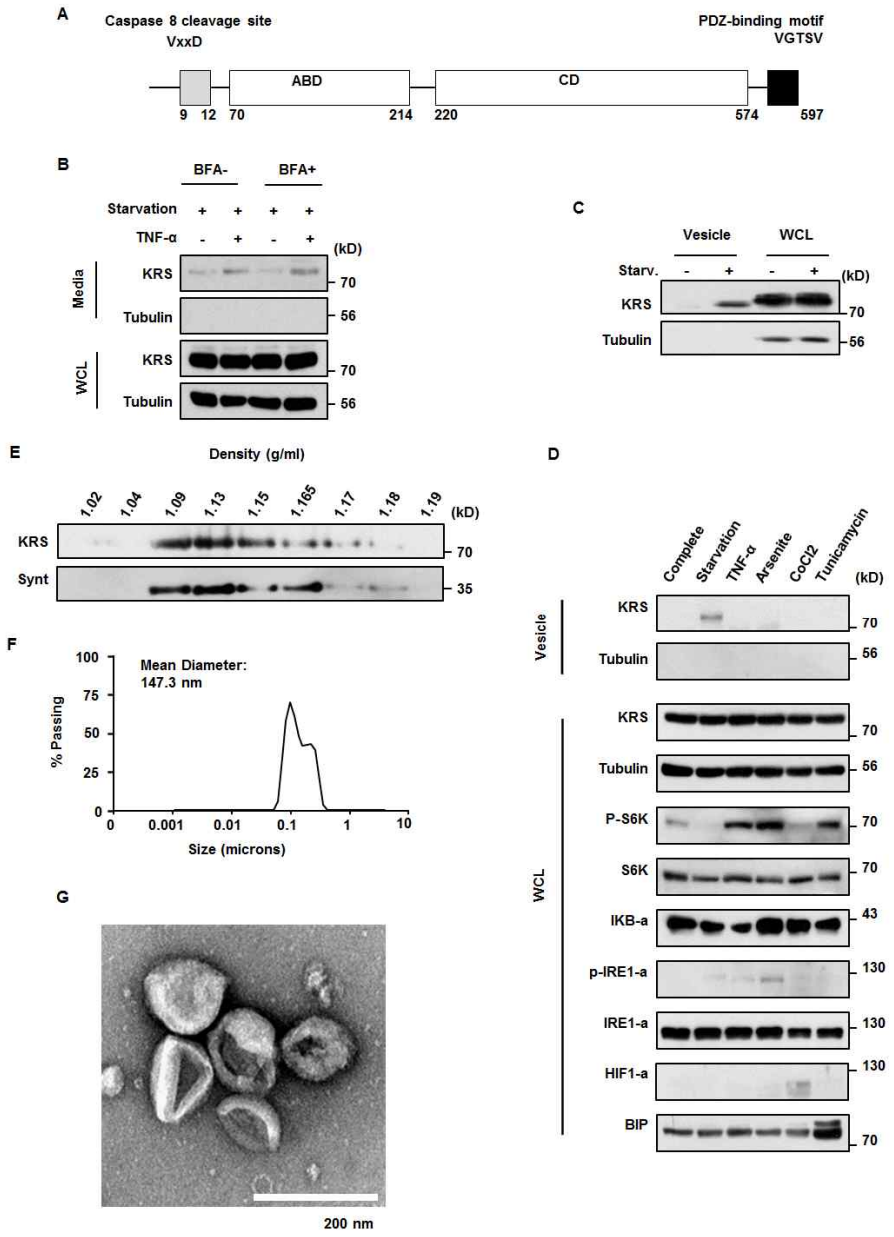

Fig. 1. KRS secretion via exosomes. (A) Human cytosolic KRS (597aa) consists of anticodon-binding (ABD, 70-214aa) and catalytic

domains (CD, 222-574aa) (Guo et al., 2008). The caspase-8 cleavage site (VxxD) and PDZ-binding motif (VGTSV) are located in the N- (9-12aa) and C-terminal (594-597aa) ends. **(B)** HCT116 cells were pre-treated with brefeldin A (2.5 mg/ml) and incubated in starvation condition with or without TNF-α (10 ng/ml). The secretion of KRS from HCT116 cells was determined by immunoblotting of KRS in harvested media after 12 h of starvation. **(C)** HCT116 cells were incubated in normal and starvation condition for 24 h. The culture medium were subjected to ultra-centrifugation at 100,000 g to obtain the pellet. KRS present in the pellets (containing vesicle fraction) was separated by 8% PAGE and detected by immunoblotting with anti-KRS antibody. Notice a slight difference in the gel mobility of KRS in the medium and cell lysates (see below for further investigation). WCL: whole cell lysates. **(D)** HCT116 cells were subjected to starvation and to treatment with TNF-α (10 ng/ml), Sodium Arsenite (12.5 mM), $CoCl_2$(100mM), and Tunicamycin (2 mg/ml) in complete media to induce inflammatory, ROS (Barchowsky et al., 1999; Ruiz-Ramos et al., 2009), Hypoxic (Piret et al., 2002) and ER stresses, respectively. Extracellular vesicles secreted into the

media were obtained by ultracentrifugation as described in Methods and the presence of KRS was determined by immunoblotting of proteins within the vesicles. **(E)** The isolated vesicles above were separated by Opti-prep gradient centrifugation. The nine fractions in the 1.02-1.19 g/ml density range were collected, and the presence of KRS and syntenin analyzed by immunoblotting with their specific antibodies. **(F)** Dynamic light scattering demonstrated the size distribution of the isolated vesicles (mean diameter: 147.3nm). **(G)** Negatively stained field of the KRS-containing vesicles isolated from HCT116 cells as above. Bar, 200 nm

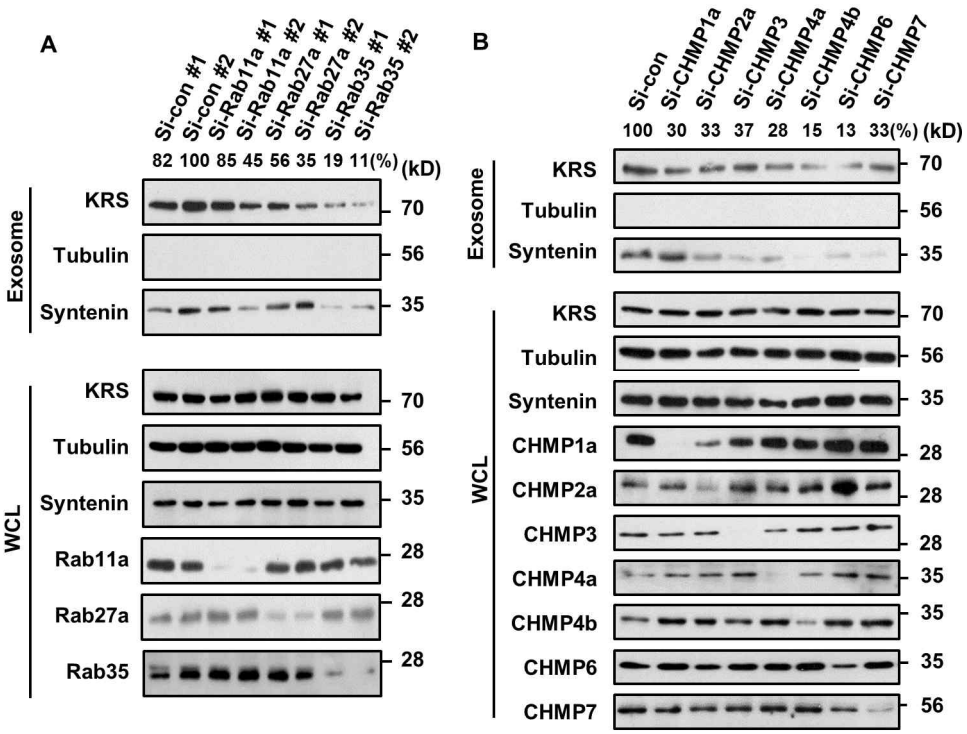

Fig. 2. KRS secreted classical exosomal pathway. (A-B) To see whether KRS exosomic secreton involved Rab (A) and ESCRT-III proteins (B), we transfected siRNAs targeting each of the indicated Rab and ESCRT-III proteins in HCT116 cells and examined whether Rab, ESCRT-III proteins affected to KRS secretion. The secretion of KRS was induced by starvation of HCT116 cells for 24 h. After isolation of the exosomes, the amounts of KRS in the obtained

exosomes were compared by immunoblotting with anti-KRS antibody. Quantitation of secreted KRS blots was measured by ImageJ.

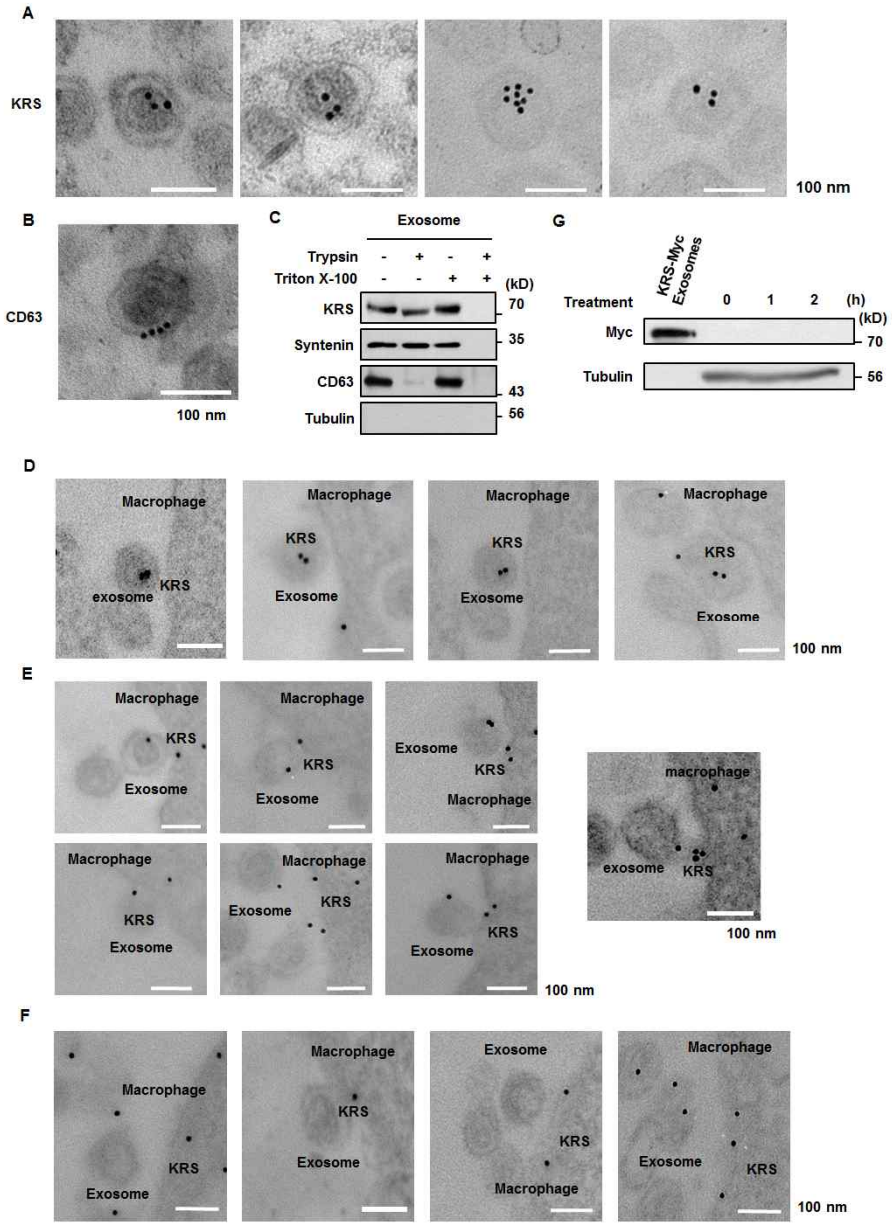

Fig. 3. KRS located inside of exosome lumen. (A-B) Localization of KRS (A) and CD63 (B), a known membrane-bound marker for

exosomes, was shown by immunogold-staining electron microscopy with their respective antibodies. Bars, 100 nm. **(C)** The isolated vesicles were incubated with or without 0.025% trypsin, 0.1% triton X-100 at 37°C for 30 min and the presence of KRS, syntenin, and CD63 was analyzed by immunoblotting with their specific antibodies. **(D-F)** Immunogold-staining electron microscopy shows KRS in the lumen of the exosome near the target macrophage (I), the release of KRS from ruptured exosomes, and uptake into the target macrophage (J and K). Bars, 100 nm. **(G)** Exosomes were isolated from HCT116 cells transfected with KRS-Myc, and incubated with macrophages. The exosome-treated macrophages were harvested at time intervals and KRS present in macrophages was then detected by immunoblotting with anti-Myc antibody to see whether KRS-Myc in the exosomes was present as the intact form.

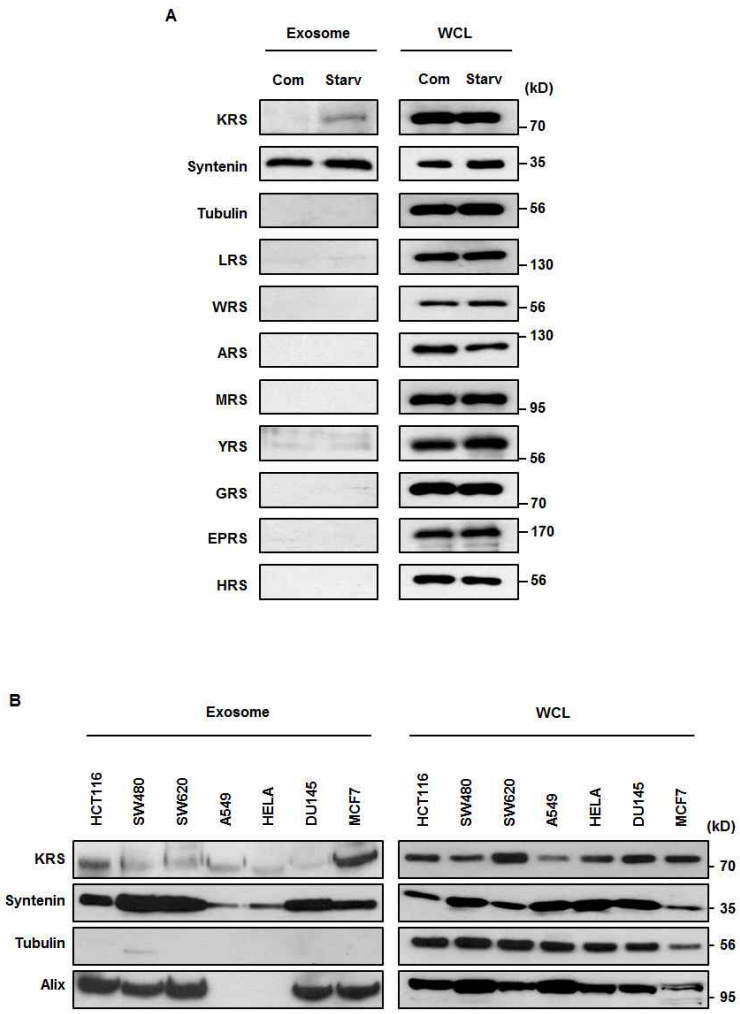

Fig. 4. Determination of exosomal secretion of ARSs and exosome secretion of KRS in different cell lines. (A) HCT116 cells were incubated in normal and starvation conditions for 24 h. The culture medium was harvested and subjected to ultra-centrifugation at 100,000 g to obtain a pellet. The presence of

different ARSs in the isolated exosomes was detected by immunoblotting with their specific antibodies. **(B)** The indicated cancer cells were incubated in starvation condition for 24 h. The culture medium was harvested and subjected to ultra-centrifugation at 100,000 g to obtain a pellet. KRS present in the isolated exosomes (10 ug total proteins) was detected by immunoblotting with anti-KRS antibody.

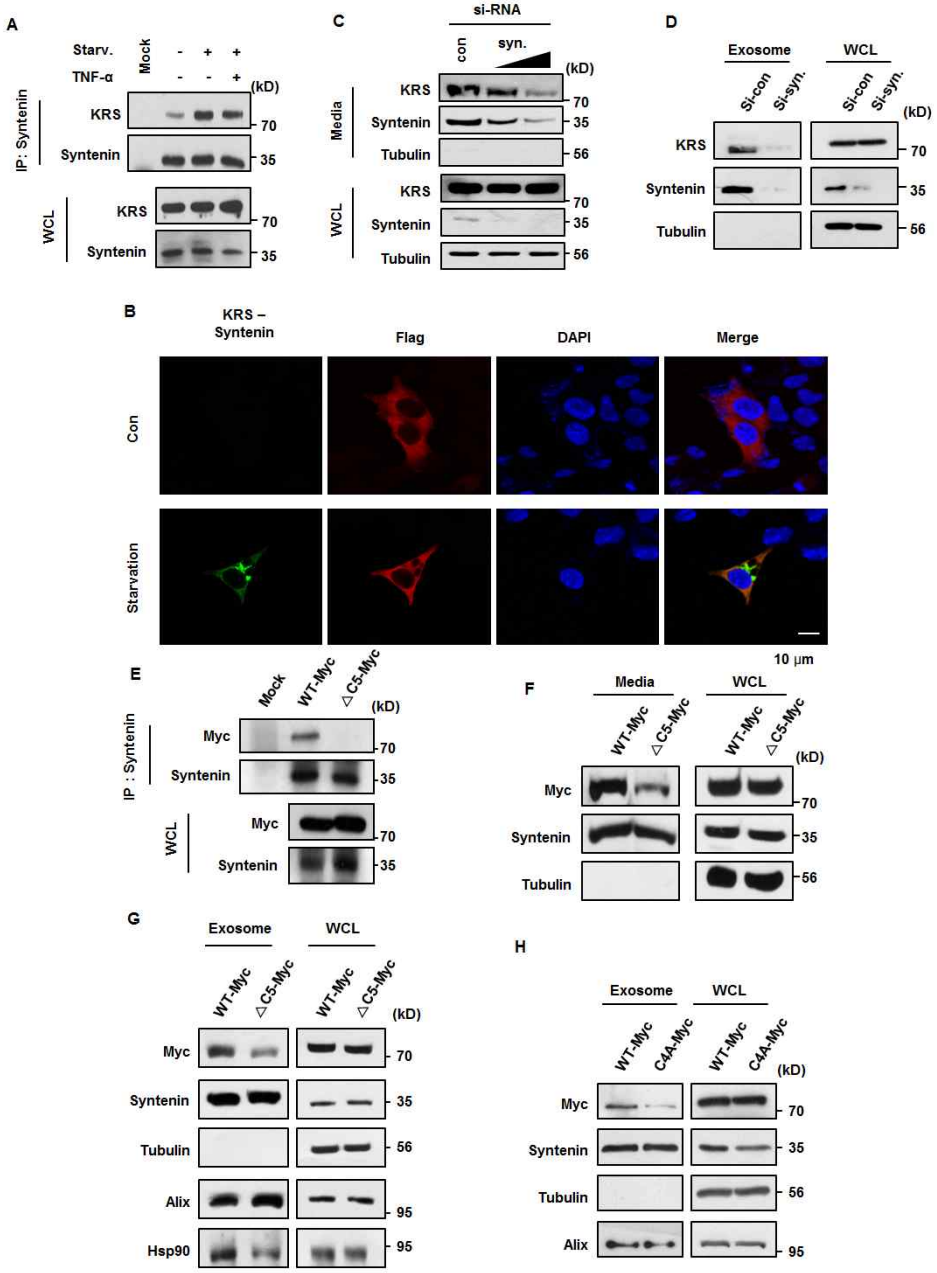

Fig. 5. Interaction of KRS with syntenin for secretion. (A) HCT116 cells were incubated in the starvation condition in the

absence and presence of TNF-α, and the interaction of KRS with syntenin was determined by co-immunoprecipitation with an anti-syntenin antibody. **(B)** The cellular interaction of KRS and syntenin was determined by Bimolecular Fluorescence Complementation (BiFC). HCT116 cells were co-transfected with Flag-KRS fused toVN173 (Venus N-terminal domain), and HA-syntenin fused to VC155 (Venus C-terminal domain). The cells were incubated in normal and starvation conditions for 6 h and reconstitution of Venus green fluorescence was shown by fluorescence microscopy. Expression of KRS was observed by red fluorescence signal from Alexa Fluor 594-conjugated anti-Flag antibody (60X). Nuclei were visualized by DAPI staining (blue). Bar, 10 mm. **(C)** Secreted KRS and syntenin were detected by immunoblotting of proteins from HCT116 cells treated with different amounts of si-RNA against syntenin. The cells were incubated in starvation condition for 24 h. Secreted proteins were precipitated with TCA and the amounts of KRS determined by immunoblotting. **(D)** The levels of KRS were also determined, as described above, in isolated exosomes and cell lysates of HCT116 cells transfected with

si-RNA against syntenin. **(E)** Interaction of KRS-Myc (WT, △C5: C-terminal 5aa deleted mutant) with syntenin was determined by co-immunoprecipitation from HCT116 cells after 1 h incubation in the starvation condition. Syntenin was precipitated from whole cell lysates with its specific antibody and the co-precipitated KRS was immunoblotted with anti-Myc antibody. **(F)** Secretion of KRS (WT, △C5) from HCT116 cells was determined in the 24 h-starvation media as above. **(G)** The amounts of KRS WT and △C5 were determined by immunoblotting in the exosomes isolated from HCT116 cells incubated in the starvation condition as above. **(H)** KRS mutant in which the last four amino acids, GTSV, were changed to alanine (C4A) was constructed. KRS WT and the C4A mutant secretion from HCT116 cells starved for 24 h, as described above, was compared.

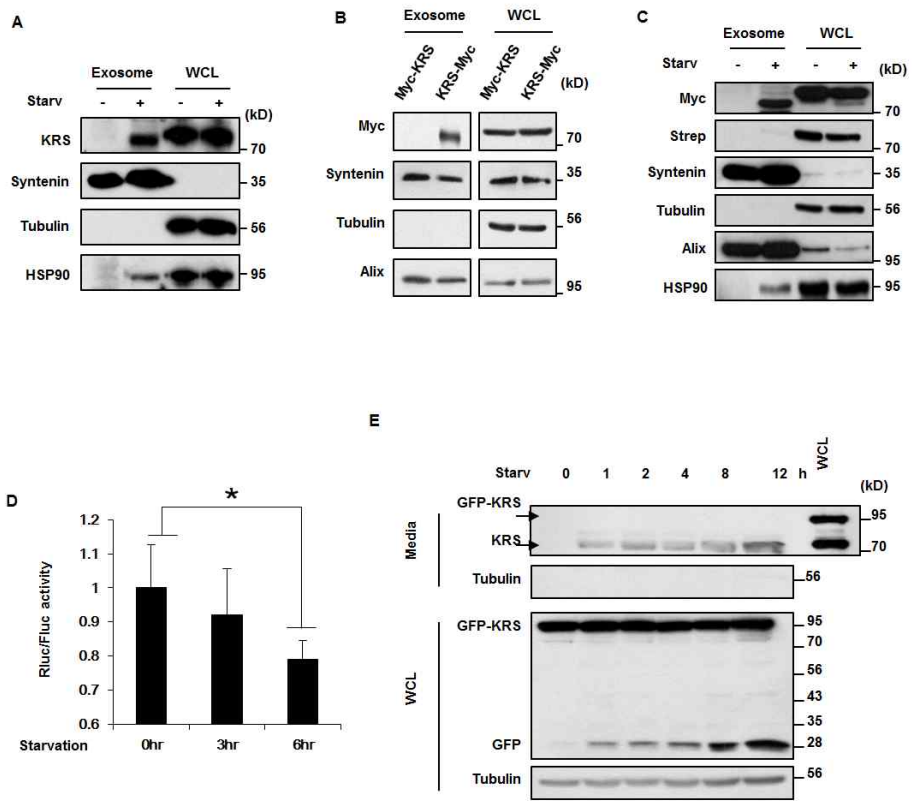

Fig. 6. The effect of an N-terminal truncation of KRS on secretion. **(A)** Secreted exosomes were isolated from the complete and starved media of HCT116 cells, and KRS in the exosomes and whole cell lysates was separated by 6% PAGE and detected by immunoblotting. **(B)** To determine the truncation site, HCT116 cells expressing either Myc-KRS (Myc tag fused to the N-terminal end of KRS) or KRS-Myc (Myc tag fused the C-terminal end of KRS)

were incubated in the starvation condition, and the exosomes were isolated from medium. KRS in the exosomes was detected with anti-Myc antibody. **(C)** HCT116 cells expressing Strep-KRS-Myc (containing Strep and Myc tags at the N- and C-terminal ends, respectively) were incubated in normal and starvation conditions for 24 h, and KRS in cytosol and exosomes was detected by immunoblotting with anti-Myc and -Strep antibodies, respectively. Syntenin, Alix, and HSP90 were used as markers for exosomes and tubulin for cytosol. **(D)** To quantify the N-terminal truncation of KRS, we fused the two domains of Renilla luciferase to each end of KRS (N-Renilla-KRS-C-Renilla) and expressed it in HCT116 cells under starvation conditions. The Renilla luciferase activities relative to those of firefly luciferase were determined at time intervals and displayed as a bar graph. n=3. *, $P<0.05$. **, $P<0.01$. **(E)** HCT116 cells expressing GFP-KRS were incubated in the starvation condition, and harvested at indicated time intervals. The amount of GFP-KRS and KRS secreted into the medium and in whole cell lysates was determined by immunoblotting with anti-KRS and -GFP antibodies, respectively.

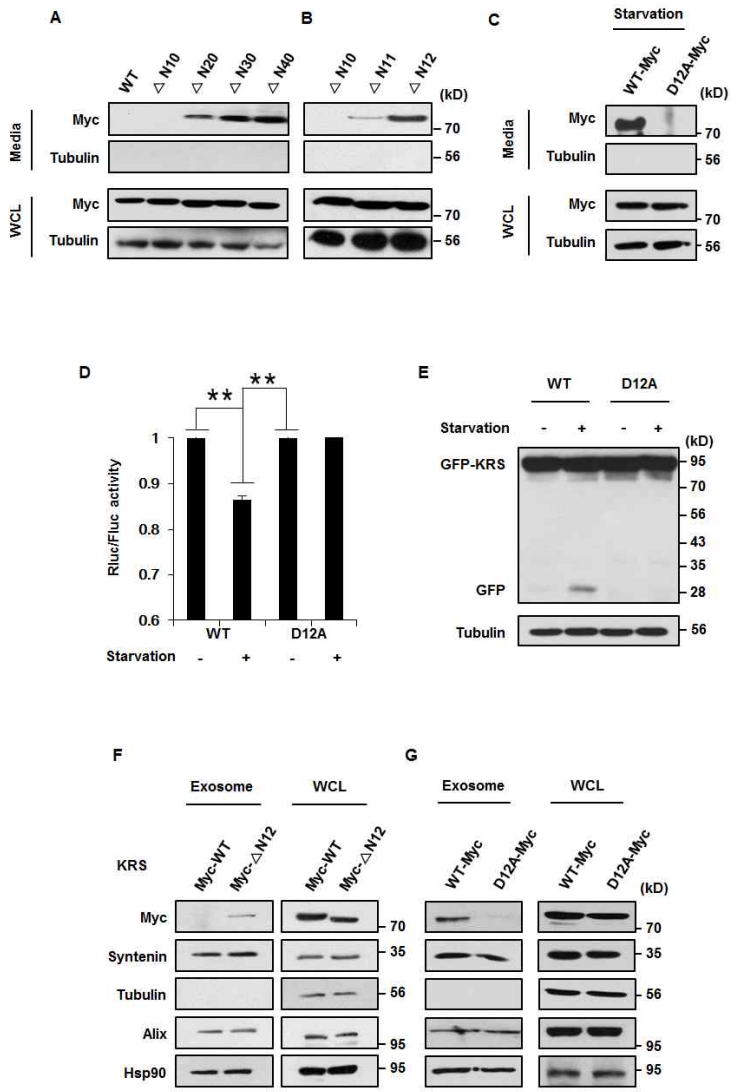

Fig. 7. Determination of KRS N-terminal truncation site. (A) HCT116 cells expressing each Myc-KRS variant (WT, △N10, △N20, △N30 and △N40) were incubated in the starvation medium for 24 h, and the secreted KRS was precipitated with TCA and subjected to

immunoblotting with anti-Myc antibody. **(B)** The same experiments were conducted with Myc-KRS △N10, △N11 and △N12. **(C)** KRS-Myc WT and D12A mutant proteins were expressed in HCT116 cells and their secretion determined by immunoblotting with anti-Myc antibody. **(D)** Effects of starvation and D12A mutation on the N-terminal cleavage of KRS were also monitored using Renilla luciferase assay as above. n=3. *, $P<0.05$. **, $P<0.01$. **(E)** Effect of D12A mutation on starvation-induced N-terminal cleavage of KRS was determined using GFP-KRS fusion protein expressed in HCT116 cells. **(F)** Myc-KRS WT and △N12 mutant were expressed in HCT116 cells and their incorporation into the secreted exosomes during 24 h starvation was determined by immunoblotting with anti-Myc antibody. **(G)** The same experiments were conducted as above with KRS WT and D12A mutant.

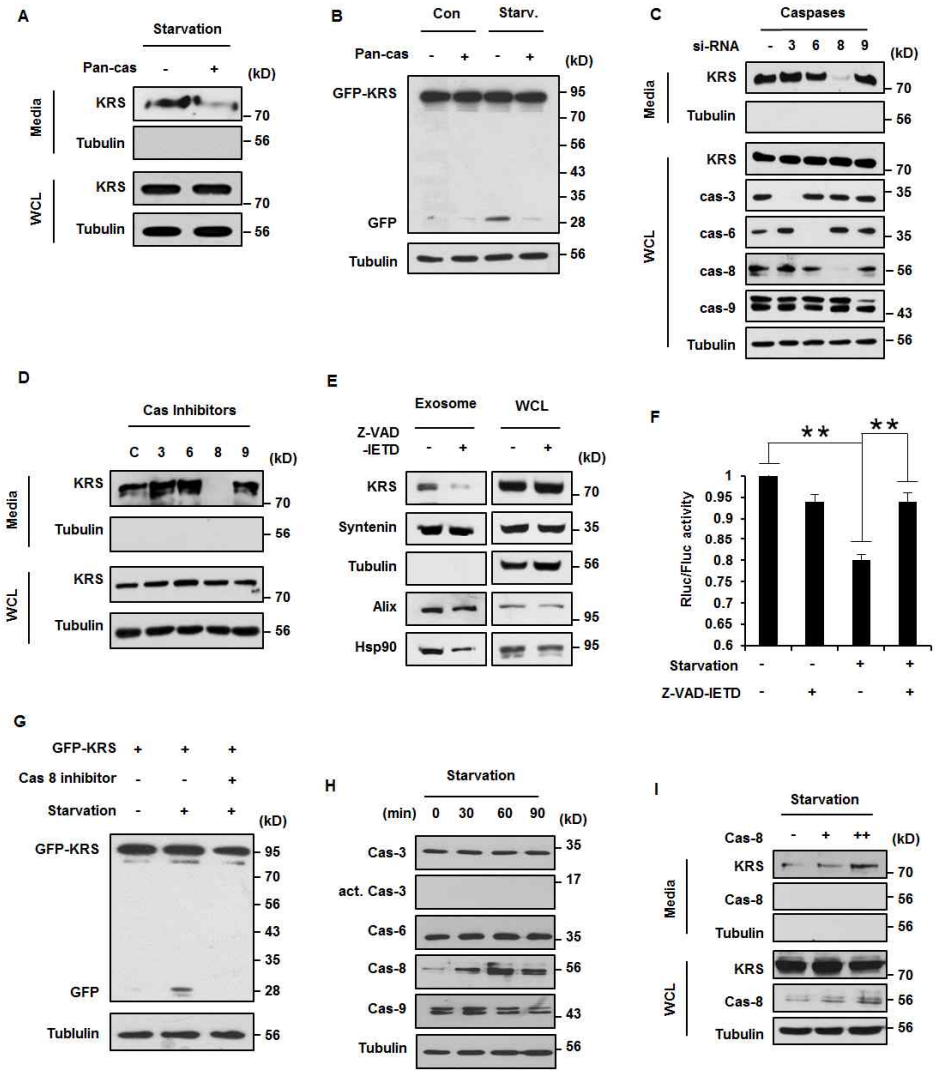

Fig. 8. N-terminal truncation of KRS by caspase-8. (A) Starved HCT116 cells were treated for 24 h with the pan-caspase inhibitor, Z-VAD-FMK, and secreted KRS was precipitated with TCA and detected by immunoblotting with anti-KRS antibody. **(B)** HCT116

cells expressing GFP-KRS were incubated in starvation medium in the absence and presence of pan-caspase inhibitor for 1 h. Cleavage of KRS was monitored by immunoblotting with anti-GFP antibody. **(C)** HCT116 cells were transfected with caspase-specific siRNAs and their effect on KRS secretion was determined by immunoblotting with anti-KRS antibody. **(D)** The starvation-induced secretion of KRS from HCT116 cells was determined by immunoblotting of the media in the presence of specific caspase inhibitors (Z-VAD-DQMD, Z-VAD-VEID, Z-VAD-IETD and Z-VAD-LEHD for caspase-3, -6, -8 and -9, respectively). Proteins in the media were precipitated with TCA and KRS levels were determined by immunoblotting with anti-KRS antibody. **(E)** The effect of a specific caspase-8 inhibitor, Z-VAD-IETD, on KRS secretion was determined by immunoblotting of the exosomes isolated. **(F)** The effect of the caspase-8 inhibitor on the N-terminal truncation of KRS was determined using KRS containing two domains of Renilla luciferase, one fused to each end. Firefly luciferase was used to monitor transfection efficiency. n=3. *, $P<0.05$. **, $P<0.01$. **(G)** HCT116 cells expressing GFP-KRS WT incubated in normal and starvation conditions were subjected to

caspase-8 inhibitor (Z-VAD-IETD) treatment for 1 h and the cleavage of GFP-KRS was determined by immunoblotting with anti-GFP antibody. **(H)** The effect of starvation on the expression levels of different caspases in HCT116 cells was determined by immunoblotting with their specific antibodies. **(I)** Different amounts of caspase-8 were expressed in the starved HCT116 cells, and its dose-dependent effect on secretion of KRS was determined.

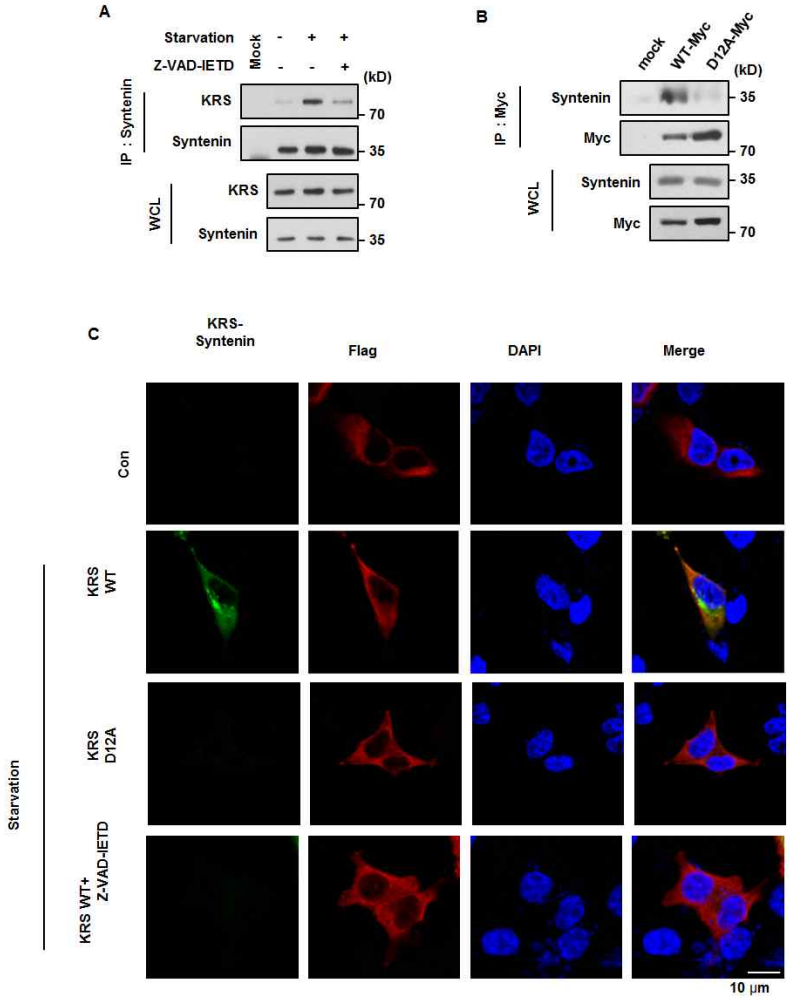

Fig. 9. N-terminal truncation of KRS is required for KRS-syntenin complex. **(A)** The effect of the caspase-8 inhibitor on the starvation-induced interaction of endogenous KRS and syntenin was determined by co-immunoprecipitation of HCT116 cell lysates using anti-syntenin and -KRS antibodies. **(B)** The effect of

the KRS D12A mutation on KRS interaction with syntenin was determined by co-immunoprecipitation. (C) The effect of caspase-8 inhibitor on the cellular interaction of the Flag-KRS (WT, D12A)-Venus (N-domain) and HA-syntenin-Venus (C-domain) in starved HCT116 cells was monitored by BiFC experiment as described above (60X). Bar, 10 mm.

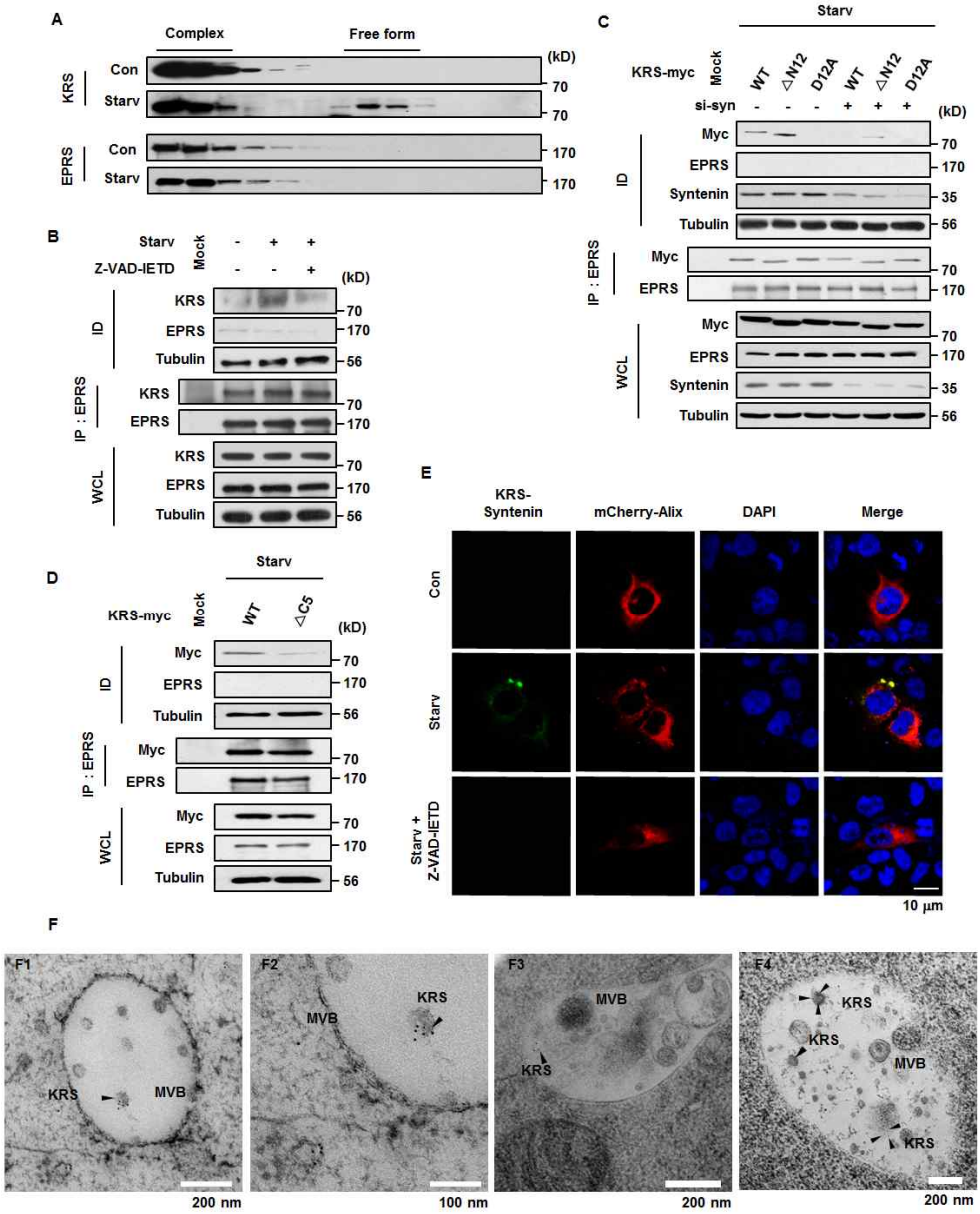

Fig. 10. Translocation of KRS from multi-tRNA synthetase complex to exosomes. (A) Dissociation of KRS and EPRS from

multi-tRNA synthetase complex (MSC) was monitored by gel filtration of proteins that were extracted from HCT116 cells incubated in the normal and starvation conditions. EPRS is a known component of MSC (Quevillon et al., 1999). **(B)** The effect of caspase-8 inhibitor (Z-VAD-ETD) on the starvation-induced dissociation of KRS from MSC in HCT116 cells was determined by co-immunoprecipitation of KRS and EPRS. The proportion of KRS dissociated from MSC was determined by immunoblotting the supernatant (ID) after removing the co-immunoprecipitates of KRS and EPRS (IP). The cellular levels of KRS and EPRS were determined in whole cell lysates (WCL). 100% and 15% of IP and ID samples were loaded for gel electrophoresis, respectively. **(C)** The effects of △N12 and D12A mutations and syntenin knockdown on the dissociation of KRS-Myc from MSC were determined as above. **(D)** The effect of △C5 (the C-terminal 5 amino acid deletion) on the dissociation of KRS-Myc from MSC were determined as above. **(E)** The effect of caspase-8 inhibitor on the association and co-localization of KRS-syntenin-Alix was shown by BiFC and fluorescence microscopy, respectively. The starvation-induced association of KRS and syntenin was shown by

BiFC (green) as described in Fig. 2B. The localization of KRS-syntenin complexes revealed by BiFC was further analyzed with mCherry-Alix (red). Nuclei were visualized by DAPI staining (blue). Bar, 10 mm. **(F)** Immunogold-staining electron microscopic analysis showing the localization of KRS in vesicles located within the multivesicular body (MVB) of HCT116 cells under starvation condition. Arrowheads in each panel indicate the localization of immunogold-labeled KRS. Bars: (F1) 200 nm, (F2) 100 nm, (F3) 200nm, (F4) 200 nm.

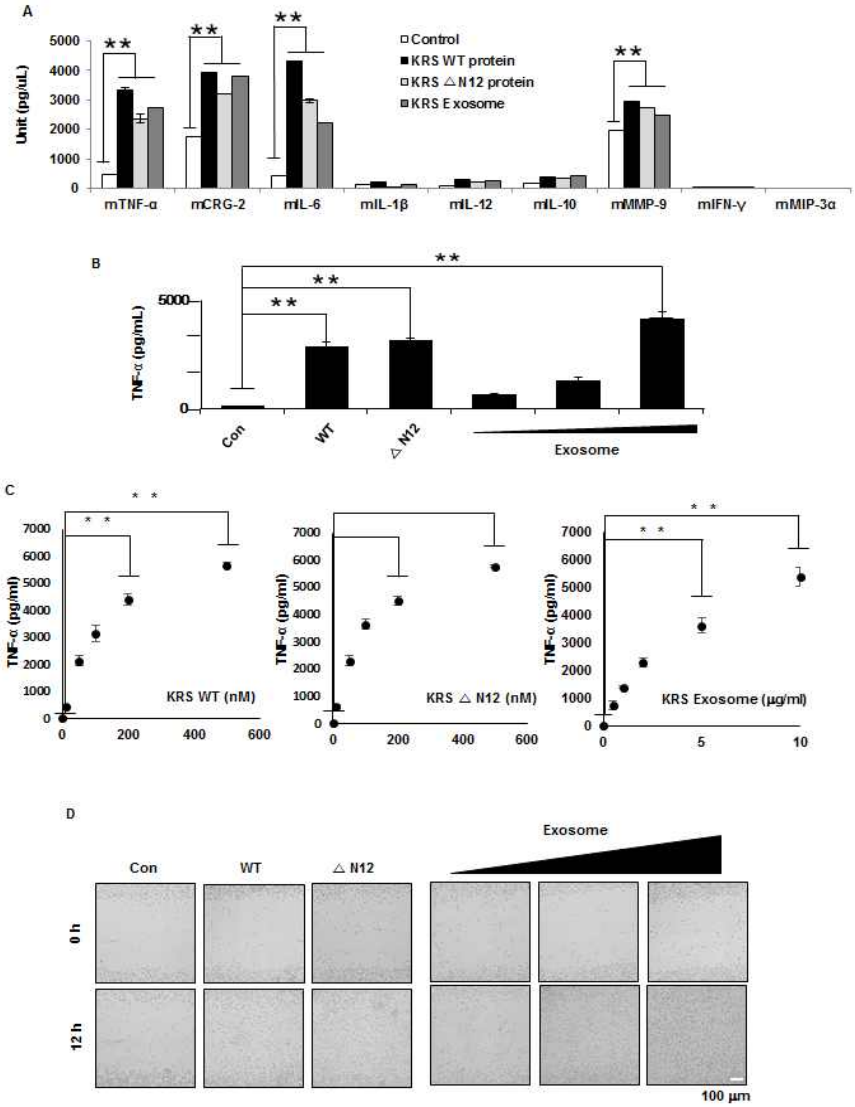

Fig. 11. Biological activities of KRS-containing exosomes. (A) Effects of KRS WT (6 mg), △N12 (6 mg) and KRS exosomes (5 mg by total proteins) on the secretion of the indicated factors from RAW 264.7 cells were determined using multiplex bead array. n=3. *, $P<0.05$. **, $P<0.01$. **(B)** The dose-dependent effect of KRS-exosomes

on the secretion of TNF-α from RAW 264.7 cells (0.1, 1 and 5 mg/ml). KRS WT and △N12 mutant (6 mg/ml) were used as the positive control. The secretion of TNF-α was quantified using a TNF-α-specific ELISA. **(C)** The dose-dependent effects of KRS WT and △N12 mutant (10, 50, 100, 200, 500nM), and KRS-exosomes (0.5, 1, 2, 5, 10 ug/ml) on the secretion of TNF-a from RAW 264.7 cells were determined. The secretion of TNF-a was quantified using a TNF-a-specific ELISA. n=3. *, $P<0.05$. **, $P<0.01$. **(D)** The effects of KRS-exosomes, and KRS WT and △N12 mutants on the migration of RAW 264.7 cells were determined by a wound-healing assay (Liang et al., 2007). RAW 264.7 cells were scratched and treated with KRS proteins (WT, △N12) and KRS-exosomes. After 12 h incubation, cell migration was monitored by microscopy. Bars, 100 mm.

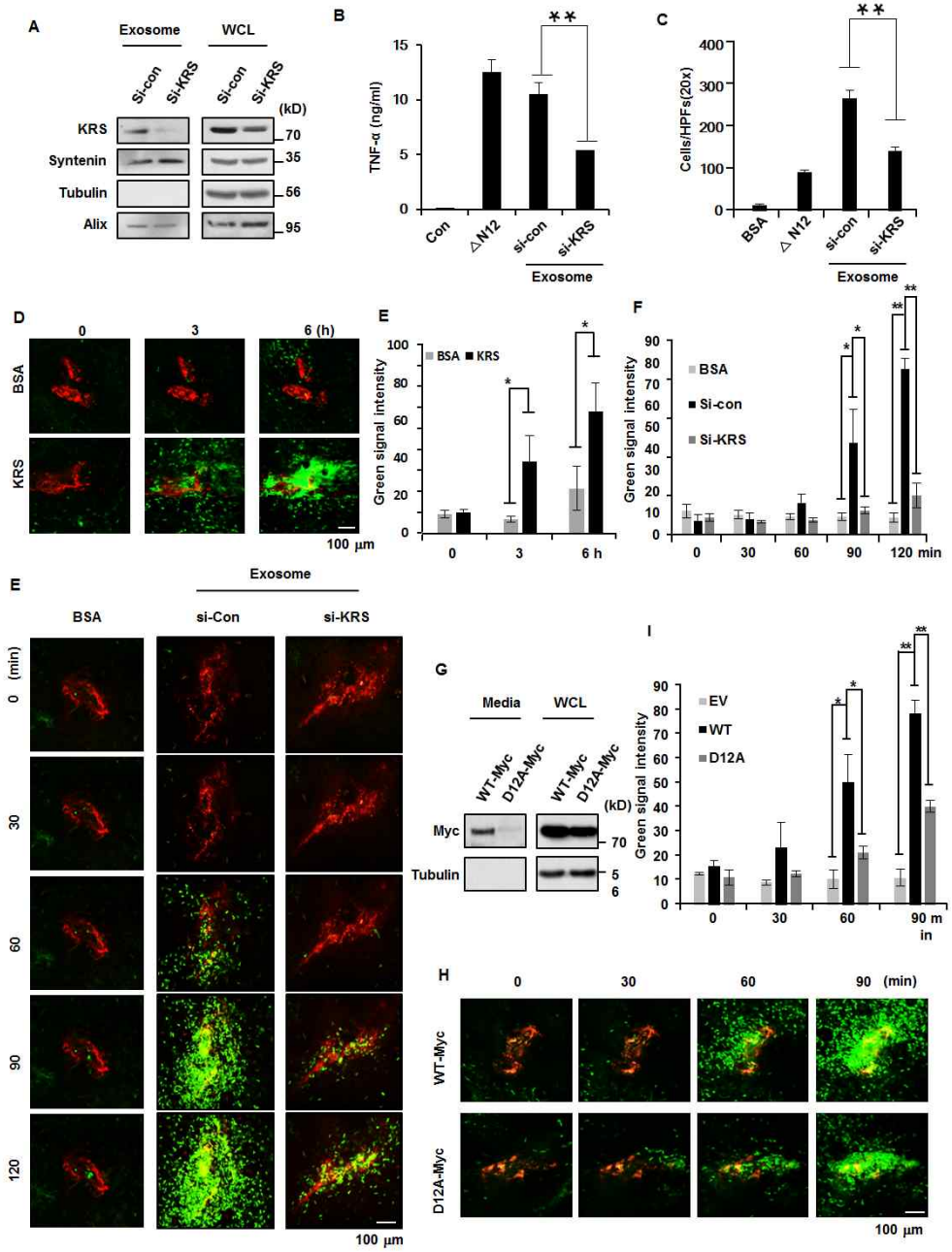

Fig. 12. KRS is essential factor for exosomal inflammatory activities. (A) To assess the functional importance of KRS for

exosomes, we reduced the KRS level in exosomes by siRNA knockdown and confirmed by immunoblotting. TNF-α-inducing **(B)** and transwell migration **(C)** activities of RAW 264.7 cells were compared for purified KRS △N12 mutant (6 mg) and exosomes (normal and KRS-suppressed, 5 mg total proteins) obtained from HCT116 cells. n=3. *, $P<0.05$. **, $P<0.01$. **(D)** KRS WT and BSA were labeled with DiI (red) and injected into mouse ear dermis (0.1 mg/ml). The recruitment of macrophages/monocytes (green) was monitored by time-lapse intravital microscopy. Bars, 100 mm. **(E)** These experiments were repeated three times and the results were represented as bar graph with standard deviation. Green fluorescence signal was measured by ImageJ. n=3. *, $P<0.05$. **, $P<0.01$. **(F)** Exosomes (normal and KRS-suppressed, 0.1 mg/ml) from HCT116 cells and bovine serum albumin (BSA) were stained with DiI (red fluorescence, (Potter et al., 1996)) and injected into mouse ear dermis. To visualize macrophage/neutrophil (green fluorescence) recruitment to the injection sites, time-lapse intravital images of macrophage/neutrophil (green fluorescence) recruitment were taken in 30 sec intervals up to 120 min after injection. Bars, 100 mm. **(G)**

These experiments were repeated three times and the results were shown as bar graph with standard deviation. Green fluorescence signal was measured by ImageJ. n=3. *, $P<0.05$. **, $P<0.01$. **(H)** The secretion of KRS from B16F10 cells expressing KRS-Myc (WT and D12A mutant) was determined by immunoblotting of harvested media. **(I-J)** B16F10 cells expressing KRS WT and D12A mutant were stained with DiD and injected into mouse ear dermis ($4x10^4$cells/ml, red fluorescence). Bars, 100 mm. These experiments were repeated three times and the results were shown as bar graph with standard deviation. Green fluorescence signal was measured by ImageJ. n=3. *, $P<0.05$. **, $P<0.01$.

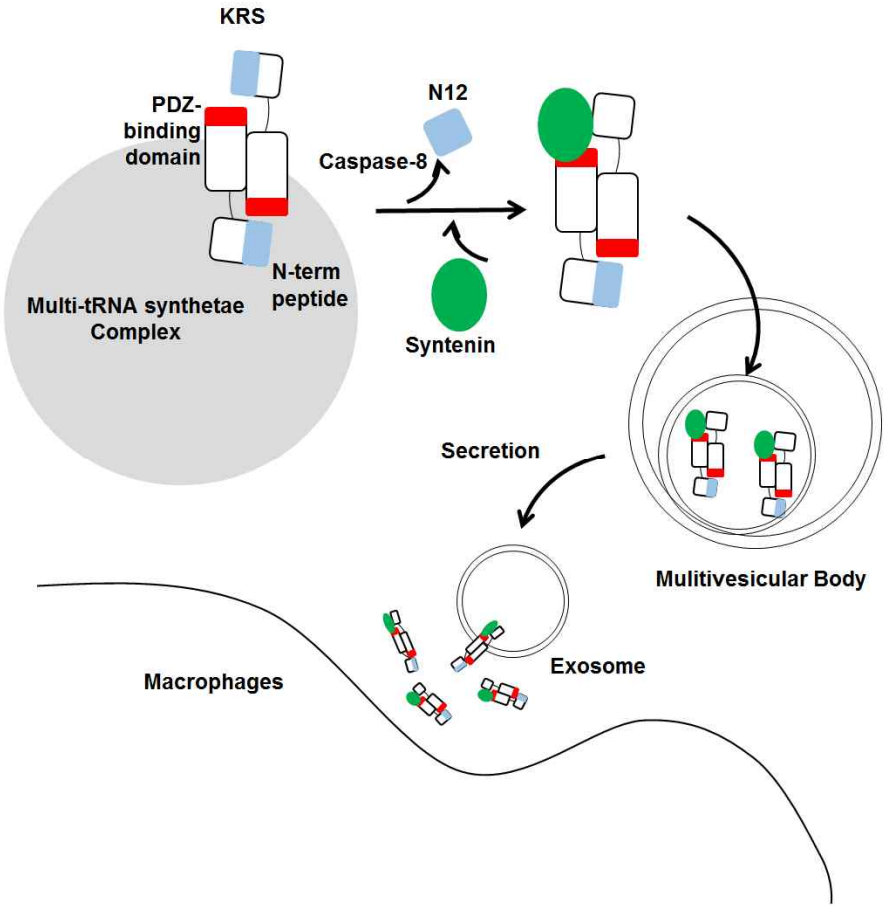

Fig. 13. Schematic working model of KRS secretion, in which two monomers of KRS bind in an antiparallel fashion to form a homodimer. In this dimer, the N-terminal 12aa of KRS (blue) blocks the exposure of the PDZ-binding motif located at the C-terminal end (red) in the counterpart monomer. Starvation-induced caspase-8 cleaves off the N-terminal 12aa to reveal the PDZ-binding motif so

that syntenin can dock. Syntenin (green) binding induces the dissociation of KRS from MSC and translocation to the MVB (multivesicular body). The KRS-containing exosomes rupture near macrophages to release KRS, which triggers macrophage activation and migration.

Discussion

Although many ARSs have been reported to be secreted (Son et al., 2014), their secretion pathways remained unanswered. In this work, we demonstrated that KRS is secreted via typical exosomes. Besides this discovery, the secretion process of KRS provides a few unexpected findings. First, a communication between the N- and C-terminal ends of KRS is functionally involved its secretion. Based on the known crystal structure of KRS in which the two monomers of KRS would exist as anti-parallel homodimer (Ofir-Birin et al., 2013), the N- and C-terminal ends of the two KRS monomers would be in close proximity through dimerization. Thus, the N-terminal peptide region of KRS might mask the PDZ-binding motif located in the C-terminal end of the other counterpart. Removal of the N-terminal peptide with caspase-8 could expose the C-terminal PDZ-binding motif of the counterpart KRS which then provides a docking site for syntenin (Fig. 13).

Second, this work suggested the third way for the KRS dissociation from MSC. So far post-translational phosphorylation has

been reported to trigger dissociation of KRS from MSC. For instance, phosphorylation at T52 and S207 was responsible for membrane and nuclear localization of KRS, respectively (Kim et al., 2012; Yannay-Cohen et al., 2009). However, it was not known how KRS is dissociated from MSC for its extracellular secretion. This work showed a new way of KRS translocation. Namely, the dissociation from MSC and extracellular secretion involve the N-terminal cleavage by caspase-8-mediated and the C-terminal interaction with syntenin.

Third, the amount of HSP90 detected in isolated exosomes showed a positive correlation with that of KRS (Fig. 5A, 5C and 7E). Considering that secreted HSP90 is also known to work as an immune stimulatory factor (Basu et al., 2000; Bohonowych et al., 2014), it is possible that KRS exerts a synergistic activity with HSP90 and other inflammatory factors present in exosomes. In fact, we determined that KRS comprised ~1% of the total exosome proteins (data not shown). Nonetheless, exosomes containing even such a low KRS content showed immune stimulatory activity comparable to the naked KRS at much higher levels (Fig. 11 and Fig.

12), supporting the notion that KRS synergizes with other exosome factors in immune cell modulation.

Fourth, we suggest a new mechanism about exosomal secretion of cytosolic proteins. There is overwhelming evidence that cytosolic proteins are present in exosome (Raposo and Stoorvogel, 2013). There are different deductions about how cytosol proteins are secreted. First, cytosolic proteins are recruited with chaperones such as HSP90, HSC70, PKM2, 14-3-3 epsilon that interact with exosomal membrane proteins. Second, lipid modifications such as palmitoylation and myristoylation of cytosolic proteins could be recruited to MVB (Buschow et al., 2010; Shen et al., 2011). However, the exact mechanism about exosomal secretion of cytosol protein is not revealed. Our data shows cytosolic KRS protein secretes through extracellular space in the syntenin dependent exosomal secretion pathway. For this mechanism, secreted KRS protein uses its two conserved sequence, N-terminal appended caspase cleavage sequence and C-terminal PDZ binding sequence. Our data shows that secreted KRS was truncated its N-terminal appended sequence by caspase-8.

KRS N-terminal truncation induced the interaction with KRS C-terminal PDZ binding domain and syntenin. When caspase-8 level was decreased using siRNA, KRS secretion was also decreased. In addition, the non-truncation mutant of KRS (D12A) secretion was also decreased. It indicates two conserved domain collaborates for KRS secretion. The exact mechanism is still unclear and further work needs to be done. With this data, this paper highlights a novel mechanism that syntenin recruits cytosolic proteins for exosomes using their PDZ domain. Furthermore, caspase-8 supports this mechanism.

Fifth, we present that caspase-8 cleavage of KRS and secreted extracellular space that induce inflammation which supports the hypothesis of caspase-8 has essential role in inflammation (Gurung and Kanneganti, 2015). Caspase-8 is involved in apoptosis induced by Fas and other apoptotic stimuli. Sequential activation of caspase-8 is the key mediator of apoptosis. But recently literatures suggested that caspase-8 play a non-apoptotic function in immune cell. Caspas-8 can directly cleave pro-IL-1β in immune cell. In our data, cancer cell increased caspase-8 in starvation condition (Figure. 8H). And

performed that caspase-8 induced KRS N-terminal truncation process. So under starvation condition, cancer cell maybe secretes KRS using caspase-8. Although we should have further work this mechanism, we showed that KRS is new target of caspase-8. Its N-terminal truncation by caspase-8 is indispensable process for secretion (Figure. 8). And induced syntenin dependent exosome secretion (Figure. 5). Finally, KRS exosomes induced by caspase-8 recruit macrophage/neutrophils and activated these immune cell that secreted TNF-alpha, IL-6, MMP9 (Figure. 11).

Syntenin is a trafficking protein using its tandem PDZ domains, which play essential role to bind to other binding partners. Syntenin is well-known adaptor protein for several transmembrane cargos. Syntenin control diverse intracellular trafficking that recycling of syndecans, biosynthetic trafficking of TGF-alpha, endocytosis of CD63 (Beekman and Coffer, 2008). KRS has PDZ binding domain in its C-terminus (Figure. 5). We speculate that syntenin could bind tetraspaniing molecualr, for example CD63, with KRS. For exosomal secretion, syntenin should bind in endosome membrane. Tetraspanin could help syntenin to bind endosome membrane. So KRS-syntenin

complex translocates MSC to endosome membrane, binds tetraspanin protein and produces ILV in MVB. Its mechanism should be solved in further work.

This KRS truncation process and interaction with syntenin is induced in starvation condition. Starvation condition induces cell cycle arrest (Rosner and Hengstschlager, 2011), (Rosner et al., 2013). KRS is one of the aminoacyl tRNA synthetase that are involved in translational machinery. Many ARSs has a non-classical role, when cells are placed in specific environment. When global translation was stopped by starvation, KRS has a potential to do non classical function. Already some ARS has a role in homeostasis regulation; we estimate that KRS also perform to regulate homeostasis. Herein, we anticipate that KRS exosome induced cancer cell apoptosis through inflammation.

The identification of KRS as a substrate of caspase-8 suggests unexpected connection of two enzymes, ARSs and caspases. While apoptotic caspases are known to initiate programmed cell death, their non-canonical activities beyond cell death have been also reported (Creagh, 2014; Man and Kanneganti, 2016). Among them, caspase-8

is shown to trigger inflammation by the activation of pro-IL1β, pro-IL18 (Bossaller et al., 2012; Gringhuis et al., 2012). However, all of these processes are known to take place in immune cells and it was not known whether caspase-8 is also involved in inflammation caused by cancers. Conversely, it remained unanswered what triggers the secretion of KRS from cancer cells to provoke inflammation. This work provides the clear answer to these unanswered questions and suggests a functional connection between caspase-mediated signaling and a key enzyme for protein synthesis for immune stimulation in extracellular space.

Materials and Methods

Cell culture and materials.

HCT116 cells were cultured in RPMI medium (with 25 mM HEPES buffer and L-glutamine, Hyclone), supplemented with 10% fetal bovine serum (FBS) and 50 μg/ml penicillin and streptomycin, at 37°C in a 5% CO_2 incubator. RAW 264.7 cells were culture din high glucose Dulbecco's modified Eagle's medium (DMEM) (with 4mM L-glutamine, 4.5 mg/ml glucose and sodium pyruvate, Hyclone),supplemented with 10% fetal bovine serum (FBS) and 50 μg/ml penicillin and streptomycin, at 37°C in a 5% CO_2 incubator. Si-RNAs specific to syntenin (SC-42164) and stealth universal RNAi (SC-37007) were purchased from SantaCruz Biotechnology, and those for KRS (HSS105656), caspase-3 (HSS101372) ,-6 (HSS101378) ,-8 (HSS141461) ,-9 (HSS189012), stealth RNAi Negative Control Medium GC Duplex (253001) were purchased from Invitrogen.They were transfected using Lipofectamine2000 Transfection reagent (Invitrogen) and X-tremeGENE HP DNA transfection reagent (Roche) following the manufacturer's protocol. The peptide inhibitors specific to

caspase-3(Z-VAD-DQMD), -6 (Z-VAD-VEID), -8 (Z-VAD-IETD) and -9 (Z-VAD-LEHD) were obtained from Calbiochem and added to cells at 14 μM in serum-free conditions.

Plasmids

The N- and C-terminal Myc-tagged human KRS proteins were cloned at the EcoRI/XhoI sites of pcDNA3 plasmid. The N-terminal one Strep tag was inserted at the KpnI/BamHI sites of the C-terminal Myc-tagged human KRS plasmid. The N-terminal Myc-tagged human KRS mutants (△N10, △N20, △N30, △N40, △N11 and △N12), and the C-terminal Myc-tagged human KRS mutants (△C5), were cloned at the EcoRI/XhoI sites of pcDNA3 plasmid. pEGFP-KRS and the BiFC plasmids of pBiFC-VN173 (Flag tag) and pBiFC-VC155 (HA tag) were previously described (Kim et al., 2012; Kwon et al., 2011). pBiFC-VN173-KRS and -VC155-syntenin were cloned at the HinDIII/XbaI (KRS), EcoRI/EcoRI (syntenin) sites of pBiFC plasmids. The BiFC N-terminal Renilla-KRS-C-terminal Renilla plasmid was a kind gift

from Dr. Min Guo (The Scripps Research Institute, Florida, USA). pmCherry-Alix plasmid was cloned at the EcoRI/BamHI sites of pmCherry-C1 plasmid. The cDNAs encoding Myc-KRS, KRS-Myc, and pBiFC-VN173-KRS mutant at D12A, C4A were cloned using a QuikChange II kit (Agilent Technologies) following the manufacturer's instruction.

Immunoblotting and immunoprecipitation

Cells were lysed with 50 mM Tris-HCl buffer (pH 7.4) containing 150 mM NaCl, 10 mM NaF, 1 mM EDTA, 1% NP-40, 10% glycerol and protease inhibitor. After 30 min, the supernatants were dissolved in SDS sample buffer and separated by SDS-PAGE. Antibodies against different ARSs were used for immunoblotting (Abcam). Antibodies specific to Hsp90 (H-114), syntenin (S-31), CD63 (H-193), Rab27a (E12A-1), GFP (B-2), Myc (9E10), caspase-3 (E-8), -6 (H-12), -8 (4.1.20), -9 (H-83), and HIF1-a (H-206) were purchased from Santa Cruz biotechnology; those for Alix (3A9), BIP (C50B12), p-S6K (Thr398, #9205), S6K (#9202), p-tyrosine (#9411), p-threonine

(#9381) and IRE1-a (14C10) were purchased from Cell Signaling Technology; p-IRE1-a (Ser724) was purchased from NOVUS biologicals; and p-serine (p3430), beta-actin (A5441) were purchased from Sigma-Aldrich. Active caspase-3 (C92-605) was purchased from BD Pharmingen. For immunoprecipitation, cells were lysed at 4°C in 50 mM HEPES buffer (pH7.4) containing 150 mM NaCl, 0.5% NP-40, 2 mM EDTA, 5% glycerol, and protease inhibitor (Calbiochem). The protein extracts were incubated with specific antibody for 2 h at 4°C with agitation, then protein G agarose was added and further incubated for 4 h. After centrifugation, the precipitated samples were resuspended in cold lysis buffer and washed 3 times. Proteins were eluted from the beads and separated by SDS-PAGE.

Determination of KRS secretion

HCT116 cells were cultivated to 60% confluency in RPMI containing 10% FBS (Hyclone). After cells were washed twice, they were transferred to serum-free RPMI for 24 h. The culture media were collected and centrifuged at 500 g for 10 min. The supernatants were

centrifuged again at 10,000 g for 30 min to eliminate membrane organelles, and then proteins were precipitated with 12% TCA and incubated for 12 h at 4 ℃. Pellets were obtained by centrifugation at 18,000 g for 15 min and neutralized with 100 mM HEPES (pH 8.0). Proteins in the pellets were separated by SDS/PAGE, and subjected to immunoblotting with an anti-KRS antibody.

Exosome isolation

Media were obtained from HCT116 cells incubated in the complete (RPMI containing 10% FBS) and starvation conditions (RPMI only) and subjected to centrifugation at 500 g for 10 min to remove cells and subsequently at 10,000 g for 30 min to remove debris. The supernatants were then centrifuged at 100,000 g for 1.5 h to precipitate exosomes. Protein content of the isolated exosomes was quantified by Bradford assay.

Opti-prep density gradient assay and dynamic light scattering

Purified exosomes were loaded onto continuous OptiPrep Density Gradient Medium (Sigma-Aldrich) (40, 20, 10 and 5% iodixanol solution with 0.25 M sucrose and 10 mM Tris-HCl, pH7.5) and centrifuged at 150,000 g for 15 h. The ten fractions were harvested and proteins in each fraction obtained by TCA precipitation. Proteins of interest were detected by immunoblot analysis. The size of the secreted vesicles was measured by an ELS-Z light scattering spectrophotometer (Otsuka Electronics, Japan).

Gel filtration chromatography

HCT116 cells were lysed with 10 mM HEPES buffer (pH 7.4) containing 10 mM KCl, 100 μM EDTA, 1 mM DTT, 0.4% Nonidet P-40 and protease inhibitor mixture. Cell lysates were centrifuged at 13,000 rpm for 15 min, and the supernatants transferred to a new tube. The supernatants (4 mg total proteins in 400 ml) were injected into a Superdex200 chromatography column 10/300 GL (GE Healthcare) in an AKTA FPLC system (Amersham Pharmacia Biotech). The separated proteins were then resolved by SDS/PAGE

and subjected to immunoblotting with antibodies specific to the indicated proteins.

Preparation of human full-length and truncated KRS

The cDNAs for human cytosolic KRS (1-597aa WT and N-terminal 12aa truncated) were subcloned into pET-28a (Novagen) with EcoRI and XhoI, and expressed in *Escherichia coli* BL21 (DE3). His-tagged KRS was then purified using nickel affinity (Invitrogen) and Mono Q ion-exchange chromatography, following the manufacturer's instructions. To remove lipopolysaccharide (LPS), the KRS solution was dialyzed in pyrogen-free buffer and subsequently filtered through Acrodisc Units with Mustang E membrane, 0.2 mm, 25 mm (Pall Corporation) in PBS containing 20% glycerol.

TNF-α ELISA assay

RAW264.7 cells ($2x10^4$) were cultured on 24-wel lplates containing DMEM with 10% FBS and 1% antibiotics for 12h, and treated with

the purified KRS at the indicated concentrations for 6h.The media were harvested after centrifugation at 3,000*g* for 5 min and the secreted TNF-α was measured using a TNF-α ELISA kit (BD Pharmingen), following the manufacturer's instruction.

BiFC immunofluorescene staining

HCT116 cells expressing KRS-VN173, syntenin-VC155, and mCherry-Alix were incubated in starvation condition with or without caspase-8 inhibitor. The cells were fixed on 9 mm coverslip with 4% paraformaldehyde and permeabilized with 0.1% Triton X-100 for 5 min and washed briefly with cold phosphate buffer saline (PBS). After a 10 min incubation with the CAS-Block (Invitrogen) for blocking, the cells were incubated for 1 h with an anti-Flag antibody. Alexa 555 (Invitrogen) was then added for 1 h at room temperature and cells DAPI stained for 10 min. After washing with cold PBS for 30 min, the specimens were observed by laser-scanning microscopy. The mounted samples were visualized at room temperature by confocal fluorescence microscope (A1 Rsi, Nikon) through an objective

lens (Plan Apochromat VC 60X, Nikon) and with NIS-Elements AR3.2 64 bit program. For live cell time-lapse microscopy, HCT116 cells expressing KRS-VN173 and syntenin-VC155 were seeded in a glass-bottom 2-well imaging chamber (Lab-Tek II, Thermo Fisher Scientific) containing RPMI with 10% FBS, and incubated using On-Stage Cell Incubation system (Live Cell Instrument) at 37 ℃ with 5% CO_2 for 12h. Cells were then starved for 3h at 37 ℃ and images were collected at 3 min intervals.The samples were visualized by confocal fluorescence microscope (A1Rsi, Nikon) through an objective lens (Plan Apochromat VC20XN. A0.75,Nikon) and EM-CCD camera (iXonEM CCD camera DU897E #BV,Andor).

Wound healing migration assay

RAW 246.7 cells ($4x10^4$) were seeded in 12-well cell culture plate in complete growth media and incubated until a confluent monolayer was formed. The monolayer of cells was wounded by manual scratching with a pipet tip, washed with PBS, and media containing either KRS WT, △N12 (6 mg/ml) protein, or KRS-exosomes (0.05,

0.5, 5 mg/ml) were added. After 12 h, the wound regions were photographed by phase contrast microscopy (C1, Nikon) through an objective lens (Plan Apo 10X), EM-CCD camera (DU-897, Andor) and with NZS-C4.11 program.

Transwell migration assay

A 24-well plate transwell chamber with 5.0 mm polycarbonate membrane (Costar) was used for cell migration assays. The inserts were coated with 10 ml of 0.5 mg/ml of gelatin (Sigma-Aldrich) and dried overnight under UV light. RAW264.7 cells were cultured in the bottom chamber. After 12 h, culture media were changed to serum-free DMEM, added to the inserts ($1x10^5$cells),and treated with BSA (100nM), KRS protein (6mg/ml), and KRS-exosomes (5 mg/ml) purified from HCT116 cells treated with control siRNA or KRS-specific siRNA for 8 h at 37 °C in a 5% CO_2 incubator. The inserts were washed twice with cold PBS and the cells fixed in 70 % methanol and 30% PBS solution for 30 min. After washing the inserts with PBS three times, the cells were fixed using hematoxylin

(Sigma-Aldrich) for 30min. The inserts were washed with distilled water three times and then on-migrant cells removed with a c ottons wab. The membranes were extracted using a blade and mounted to amicroslide using GelMount (Biomeda). Images of the migrating cells were taken with Optical microscope (20X, KoreaLabTech) using the Topview 3.5program.

Intravital imaging

A custom-built laser-scanning confocal microscope modified from a previously constructed system (Choe et al., 2013) was used to visualize macrophage/neutrophil recruitment. Three CW lasers at 488 nm (MLD488 60 mW, Cobolt), 561 nm (Jive 50 mW, Cobolt) and 640 nm (MLD640 100 mW, Cobolt) were used as excitation source. To implement 2D scanning, a fast-rotating polygonal mirror (MC-5, aluminum coated, Lincoln Laser) and galvanometer (6230H, Cambridge Technology) were used. High-sensitivity photomultiplier tubes (R9110, Hamamatsu) were used to detect three-color fluorescence signals simultaneously. Three detection channels were split by dichroic

mirrors (FF01-442/46-25, FF02-525/50-25, FF01-585/40-25, FF01-685/40-25, Semrock) and bandpass filters (FF484-FDi01, FF560-Di01, FF649-Di01, Semrock). Electric signals obtained from photomultiplier tube were digitized by an 8-bit 3-channel frame grabber (Solios, Matrox). The field of view (FOV) of images obtained by the 20X objective (LUMFLN60XW, NA1.1, Olympus) was 500x500 μm^2. After acquisition from the imaging system, 512x512 pixel images were then XY-shift compensated with Matlab (Mathworks). During the imaging, a motorized XYZ translational stage (MPC-200-ROE, Sutter Instrument), which has 1μm resolution, was used to precisely adjust sample position.

LysM-GFP (Lysozyme M-GFP) mice (Faust et al., 2000) that endogenously express GFP in macrophages and neutrophils were used. 12-20 week old male LysM-GFP mice were deeply anaesthetized with intraperitoneal injection of Zoletil (30 mg/kg) and Rompun (10 mg/kg). During imaging, mouse body temperature was maintained at 37°C with a homoeothermic controller (PhysioSuite, RightTemp, Kent Scientific). To avoid immune responses caused by

hair removal, mouse ear skin was shaved at least 12 h before imaging.

B16F10 cells were transfected with myc-KRS, KRS-Myc (WT and D12A Mutant) and empty vector using Lipofectamine 2000 (Invitrogen). The transfected B16F10 cells were then fluorescently labeled with the lipophilic fluorescent dye, Vybrant DiI, or DiD solution (Thermo Fisher Scientific) by incubating with 5 μl of DiI or DiD solution per ml of cell media for 1 h. After washing with PBS three times, labeled cells were prepared in PBS solution and intradermally injected into mouse ear skin ($4x10^4$cells/μl) with a 31 G microinjector. To visualize macrophage/neutrophil recruitment along the cell injection site, time-lapse images were taken at 30 sec intervals after injection.

HCT116 cells were transfected with control siRNA (Si-con) and KRS-specific siRNA (si-KRS) using X-tremeGENE HP DNA transfection reagent (Roche), following the manufacturer's protocol. The transfected HCT116 cells were incubated with DiI (5 μl/ml) for 1 h. After washing with PBS, the labeled cells were incubated in starvation condition for 24 h. Si-con, si-KRS exosomes were purified

from incubation media using the exosome isolation method described above. Exosomes were intradermally injected into mouse ear skin (0.1 μg/μl) with 31 G microinjector. Time-lapse images were taken at 30 sec intervals after injection.

Luminex screening assays (bead-based multiplex kits)

RAW 246.7 cells were cultured in 12-well plate in DMEM with 10% FBS and 1% antibiotics for 12 h and starved in serum-free media for 2 h. Different amounts of KRS (WT and △N12 mutant, 6 mg/ml) and KRS-exosomes (5 mg/ml) were added to the media. At different time intervals, the media were collected and subjected to centrifugation at 3,000 g for 10 min. For the multiplex assay, the secretion of TNF-α, mCRG-2, IL-6, mIL-1b, mIL-12, mIL-10, MMP9, INF-ɣ, mMIP3a and CXCL10 was measured using premixed beads purchased from R&D Science, following manufacturer's instructions, and quantified by BioRad Bioplex 200 system and software.

Renilla BiFC luciferase assay

BiFC Renilla luciferase KRS vector (provided by Dr. Min Guo, The Scripps Research Institute, Florida, USA), which the N- and C-terminal domains of Renilla luciferase were fused to the N- and C-terminal ends of KRS, was co-transfected into HCT116 cells, along with the firefly luciferase vector. After 24 h, cells were incubated in each starvation condition with or without caspase-8 inhibitor. Luciferase activity was measured using a luciferase assay kit (Promega) and luminometer.

Immunogold-label electron microscopy

Exosomes isolated from starved HCT116 cells and exosome-treated macrophages were fixed with 2.5% glutaaldehyde and 2% osmium tetroxide for 1 h at 4 °C. They were then dehydrated with a graded acetone series and embedded into Spurr's medium (EMS). The sections were made in 60 nm thickness horizontally to the plane of the samples using an ultramicrotome (RMC MTXL) and mounted on nickel grids. Free aldehyde groups were quenched with 0.02 M glycine for 10 min. Sections were then rinsed in deionized water,

floated for 1 h in PBS containing 1% BSA, and incubated directly in the primary rabbit antibodies at 4°C for 1 h. Sections were rinsed several times with PBS-BSA (0.1% BSA in PBS) and floated for 1 h in the rabbit IgG conjugated to 10 nm gold particles (Sigma-Aldrich) diluted 1:50 in PBS-BSA. The gold particle-labelled sections were counterstained with uranyl acetate and lead citrate. For immunogold staining of KRS in multivesicular body (MVB), HCT116 cells were incubated in serum free RPMI1640 medium for 3 h, and then cells collected by low-speed centrifugation. Following the preparative steps of cryo-fixation (Donohoe et al., 2007), the prepared sections were examined using a Hitachi H-7600 (Hitachi, operating at at 80 k) and a JEM-1400 PLUS Transmission Electron Microscope (JEOL)

Statistical methods

The Student's t-test was used for statistical anlaysis. P-value <0.05 was considered a statistically significant result.

.

References

Baietti, M.F., Z. Zhang, E. Mortier, A. Melchior, G. Degeest, A. Geeraerts, Y. Ivarsson, F. Depoortere, C. Coomans, E. Vermeiren, P. Zimmermann, and G. David. 2012. Syndecan-syntenin-ALIX regulates the biogenesis of exosomes. *Nat. Cell Biol.* 14:677-685.

Barchowsky, A., L.R. Klei, E.J. Dudek, H.M. Swartz, and P.E. James. 1999. Stimulation of reactive oxygen, but not reactive nitrogen species, in vascular endothelial cells exposed to low levels of arsenite. *Free Radic. Biol. Med.* 27:1405-1412.

Basu, S., R.J. Binder, R. Suto, K.M. Anderson, and P.K. Srivastava. 2000. Necrotic but not apoptotic cell death releases heat shock proteins, which deliver a partial maturation signal to dendritic cells and activate the NF-kappa B pathway. *Int. Immunol.* 12:1539-1546.

Bohonowych, J.E., M.W. Hance, K.D. Nolan, M. Defee, C.H. Parsons, and J.S. Isaacs. 2014. Extracellular Hsp90 mediates an NF-kappaB dependent inflammatory stromal program: implications for the prostate tumor microenvironment. *Prostate.* 74:395-407.

Bossaller, L., P.I. Chiang, C. Schmidt-Lauber, S. Ganesan, W.J. Kaiser, V.A. Rathinam, E.S. Mocarski, D. Subramanian, D.R. Green, N. Silverman, K.A. Fitzgerald, A. Marshak-Rothstein, and E. Latz. 2012. Cutting edge: FAS (CD95) mediates

noncanonical IL-1beta and IL-18 maturation via caspase-8 in an RIP3-independent manner. *J. Immunol.* 189:5508-5512.

Choe, K., Y. Hwang, H. Seo, and P. Kim. 2013. In vivo high spatiotemporal resolution visualization of circulating T lymphocytes in high endothelial venules of lymph nodes. *J Biomed Opt.* 18:036005.

Choi, J.W., D.G. Kim, A.E. Lee, H.R. Kim, J.Y. Lee, N.H. Kwon, Y.K. Shin, S.K. Hwang, S.H. Chang, M.H. Cho, Y.L. Choi, J. Kim, S.H. Oh, B. Kim, S.Y. Kim, H.S. Jeon, J.Y. Park, H.P. Kang, B.J. Park, J.M. Han, and S. Kim. 2011. Cancer-associated splicing variant of tumor suppressor AIMP2/p38: pathological implication in tumorigenesis. *PLoS Genet.* 7:e1001351.

Creagh, E.M. 2014. Caspase crosstalk: integration of apoptotic and innate immune signalling pathways. *Trends Immunol.* 35:631-640.

Donohoe, B.S., B.H. Kang, and L.A. Staehelin. 2007. Identification and characterization of COPIa- and COPIb-type vesicle classes associated with plant and algal Golgi. *Proc. Natl. Acad. Sci. U. S. A.* 104:163-168.

Fabre, S., C. Reynaud, and P. Jalinot. 2000. Identification of functional PDZ domain binding sites in several human proteins. *Mol. Biol. Rep.* 27:217-224.

Faust, N., F. Varas, L.M. Kelly, S. Heck, and T. Graf. 2000. Insertion of enhanced green fluorescent protein into the lysozyme gene

creates mice with green fluorescent granulocytes and macrophages. *Blood*. 96:719-726.

Gringhuis, S.I., T.M. Kaptein, B.A. Wevers, B. Theelen, M. van der Vlist, T. Boekhout, and T.B. Geijtenbeek. 2012. Dectin-1 is an extracellular pathogen sensor for the induction and processing of IL-1beta via a noncanonical caspase-8 inflammasome. *Nat. Immunol.* 13:246-254.

Guo, M., M. Ignatov, K. Musier-Forsyth, P. Schimmel, and X.L. Yang. 2008. Crystal structure of tetrameric form of human lysyl-tRNA synthetase: Implications for multisynthetase complex formation. *Proc. Natl. Acad. Sci. U. S. A.* 105:2331-2336.

Guo, M., and P. Schimmel. 2013. Essential nontranslational functions of tRNA synthetases. *Nat. Chem. Biol.* 9:145-153.

Guo, M., P. Schimmel, and X.L. Yang. 2010. Functional expansion of human tRNA synthetases achieved by structural inventions. *FEBS Lett.* 584:434-442.

Han, J.M., S.G. Park, B. Liu, B.J. Park, J.Y. Kim, C.H. Jin, Y.W. Song, Z. Li, and S. Kim. 2007. Aminoacyl-tRNA synthetase-interacting multifunctional protein 1/p43 controls endoplasmic reticulum retention of heat shock protein gp96: its pathological implications in lupus-like autoimmune diseases. *Am. J. Pathol.* 170:2042-2054.

Hsu, C., Y. Morohashi, S. Yoshimura, N. Manrique-Hoyos, S. Jung, M.A. Lauterbach, M. Bakhti, M. Gronborg, W. Mobius, J. Rhee,

F.A. Barr, and M. Simons. 2010. Regulation of exosome secretion by Rab35 and its GTPase-activating proteins TBC1D10A-C. *J. Cell Biol.* 189:223-232.

Ibba, M., and D. Soll. 2000. Aminoacyl-tRNA synthesis. *Annu. Rev. Biochem.* 69:617-650

Kerppola, T.K. 2008. Bimolecular fluorescence complementation (BiFC) analysis as a probe of protein interactions in living cells. *Annu Rev Biophys.* 37:465-487.

Kim, D.G., J.W. Choi, J.Y. Lee, H. Kim, Y.S. Oh, J.W. Lee, Y.K. Tak, J.M. Song, E. Razin, S.H. Yun, and S. Kim. 2012. Interaction of two translational components, lysyl-tRNA synthetase and p40/37LRP, in plasma membrane promotes laminin-dependent cell migration. *FASEB J.* 26:4142-4159.

Kim, D.G., J.Y. Lee, N.H. Kwon, P. Fang, Q. Zhang, J. Wang, N.L. Young, M. Guo, H.Y. Cho, A.U. Mushtaq, Y.H. Jeon, J.W. Choi, J.M. Han, H.W. Kang, J.E. Joo, Y. Hur, W. Kang, H. Yang, D.H. Nam, M.S. Lee, J.W. Lee, E.S. Kim, A. Moon, K. Kim, D. Kim, E.J. Kang, Y. Moon, K.H. Rhee, B.W. Han, J.S. Yang, G. Han, W.S. Yang, C. Lee, M.W. Wang, and S. Kim. 2014. Chemical inhibition of prometastatic lysyl-tRNA synthetase-laminin receptor interaction. *Nat. Chem. Biol.* 10:29-34.

Kwon, N.H., T. Kang, J.Y. Lee, H.H. Kim, H.R. Kim, J. Hong, Y.S. Oh, J.M. Han, M.J. Ku, S.Y. Lee, and S. Kim. 2011. Dual role of methionyl-tRNA synthetase in the regulation of translation

and tumor suppressor activity of aminoacyl-tRNA synthetase-interacting multifunctional protein-3. *Proc. Natl. Acad. Sci. U. S. A.* 108:19635-19640.

Lacy, P., and J.L. Stow. 2011. Cytokine release from innate immune cells: association with diverse membrane trafficking pathways. *Blood.* 118:9-18.

Liang, C.C., A.Y. Park, and J.L. Guan. 2007. In vitro scratch assay: a convenient and inexpensive method for analysis of cell migration in vitro. *Nat Protoc.* 2:329-333.

Man, S.M., and T.D. Kanneganti. 2016. Converging roles of caspases in inflammasome activation, cell death and innate immunity. *Nat. Rev. Immunol.* 16:7-21.

Manes, S., G. Fuentes, R.M. Peregil, A.M. Rojas, and R.A. Lacalle. 2010. An isoform-specific PDZ-binding motif targets type I PIP5 kinase beta to the uropod and controls polarization of neutrophil-like HL60 cells. *FASEB J.* 24:3381-3392.

Mantovani, A., S. Sozzani, M. Locati, P. Allavena, and A. Sica. 2002. Macrophage polarization: tumor-associated macrophages as a paradigm for polarized M2 mononuclear phagocytes. *Trends Immunol.* 23:549-555.

Marzesco, A.M., P. Janich, M. Wilsch-Brauninger, V. Dubreuil, K. Langenfeld, D. Corbeil, and W.B. Huttner. 2005. Release of extracellular membrane particles carrying the stem cell marker prominin-1 (CD133) from neural progenitors and other epithelial cells. *J. Cell. Sci.* 118:2849-2858.

Matsuo, H., J. Chevallier, N. Mayran, I. Le Blanc, C. Ferguson, J. Faure, N.S. Blanc, S. Matile, J. Dubochet, R. Sadoul, R.G. Parton, F. Vilbois, and J. Gruenberg. 2004. Role of LBPA and Alix in multivesicular liposome formation and endosome organization. *Science*. 303:531-534.

Meerschaert, K., E. Remue, A. De Ganck, A. Staes, C. Boucherie, K. Gevaert, J. Vandekerckhove, L. Kleiman, and J. Gettemans. 2008. The tandem PDZ protein Syntenin interacts with the aminoacyl tRNA synthetase complex in a lysyl-tRNA synthetase-dependent manner. *J Proteome Res*. 7:4962-4973.

Mirando, A.C., C.S. Francklyn, and K.M. Lounsbury. 2014. Regulation of angiogenesis by aminoacyl-tRNA synthetases. *Int J Mol Sci*. 15:23725-23748.

Nechushtan, H., S. Kim, G. Kay, and E. Razin. 2009. Chapter 1: The physiological role of lysyl tRNA synthetase in the immune system. *Adv. Immunol*. 103:1-27.

Odorizzi, G. 2006. The multiple personalities of Alix. *J. Cell. Sci*. 119:3025-3032.

Ofir-Birin, Y., P. Fang, S.P. Bennett, H.M. Zhang, J. Wang, I. Rachmin, R. Shapiro, J. Song, A. Dagan, J. Pozo, S. Kim, A.G. Marshall, P. Schimmel, X.L. Yang, H. Nechushtan, E. Razin, and M. Guo. 2013. Structural switch of lysyl-tRNA synthetase between translation and transcription. *Mol. Cell*. 49:30-42.

Ostrowski, M., N.B. Carmo, S. Krumeich, I. Fanget, G. Raposo, A. Savina, C.F. Moita, K. Schauer, A.N. Hume, R.P. Freitas, B.

Goud, P. Benaroch, N. Hacohen, M. Fukuda, C. Desnos, M.C. Seabra, F. Darchen, S. Amigorena, L.F. Moita, and C. Thery. 2010. Rab27a and Rab27b control different steps of the exosome secretion pathway. *Nat. Cell Biol.* 12:19-30; sup pp 11-13.

Park, B.J., J.W. Kang, S.W. Lee, S.J. Choi, Y.K. Shin, Y.H. Ahn, Y.H. Choi, D. Choi, K.S. Lee, and S. Kim. 2005a. The haploinsufficient tumor suppressor p18 upregulates p53 via interactions with ATM/ATR. *Cell.* 120:209-221.

Park, M.C., T. Kang, D. Jin, J.M. Han, S.B. Kim, Y.J. Park, K. Cho, Y.W. Park, M. Guo, W. He, X.L. Yang, P. Schimmel, and S. Kim. 2012. Secreted human glycyl-tRNA synthetase implicated in defense against ERK-activated tumorigenesis. *Proc. Natl. Acad. Sci. U. S. A.* 109:E640-647.

Park, S.G., H.J. Kim, Y.H. Min, E.C. Choi, Y.K. Shin, B.J. Park, S.W. Lee, and S. Kim. 2005b. Human lysyl-tRNA synthetase is secreted to trigger proinflammatory response. *Proc. Natl. Acad. Sci. U. S. A.* 102:6356-6361.

Park, S.G., H. Shin, Y.K. Shin, Y. Lee, E.C. Choi, B.J. Park, and S. Kim. 2005c. The novel cytokine p43 stimulates dermal fibroblast proliferation and wound repair. *Am. J. Pathol.* 166:387-398.

Piret, J.P., D. Mottet, M. Raes, and C. Michiels. 2002. CoCl2, a chemical inducer of hypoxia-inducible factor-1, and hypoxia

reduce apoptotic cell death in hepatoma cell line HepG2. *Ann. N. Y. Acad. Sci.* 973:443-447.

Potter, S.M., C.M. Wang, P.A. Garrity, and S.E. Fraser. 1996. Intravital imaging of green fluorescent protein using two-photon laser-scanning microscopy. *Gene.* 173:25-31.

Quevillon, S., J.C. Robinson, E. Berthonneau, M. Siatecka, and M. Mirande. 1999. Macromolecular assemblage of aminoacyl-tRNA synthetases: identification of protein-protein interactions and characterization of a core protein. *J. Mol. Biol.* 285:183-195.

Rosa, P., F.A. Barr, J.C. Stinchcombe, C. Binacchi, and W.B. Huttner. 1992. Brefeldin A inhibits the formation of constitutive secretory vesicles and immature secretory granules from the trans-Golgi network. *Eur. J. Cell Biol.* 59:265-274.

Ruiz-Ramos, R., L. Lopez-Carrillo, A.D. Rios-Perez, A. De Vizcaya-Ruiz, and M.E. Cebrian. 2009. Sodium arsenite induces ROS generation, DNA oxidative damage, HO-1 and c-Myc proteins, NF-kappaB activation and cell proliferation in human breast cancer MCF-7 cells. *Mutat. Res.* 674:109-115.

Sampath, P., B. Mazumder, V. Seshadri, C.A. Gerber, L. Chavatte, M. Kinter, S.M. Ting, J.D. Dignam, S. Kim, D.M. Driscoll, and P.L. Fox. 2004. Noncanonical function of glutamyl-prolyl-tRNA synthetase: gene-specific silencing of translation. *Cell.* 119:195-208.

Savina, A., C.M. Fader, M.T. Damiani, and M.I. Colombo. 2005. Rab11 promotes docking and fusion of multivesicular bodies in a calcium-dependent manner. *Traffic*. 6:131-143.

Son, S.H., M.C. Park, and S. Kim. 2014. Extracellular activities of aminoacyl-tRNA synthetases: new mediators for cell-cell communication. *Top Curr Chem*. 344:145-166.

Sutton, E.J., T.D. Henning, B.J. Pichler, C. Bremer, and H.E. Daldrup-Link. 2008. Cell tracking with optical imaging. *Eur Radiol*. 18:2021-2032.

Thery, C., M. Ostrowski, and E. Segura. 2009. Membrane vesicles as conveyors of immune responses. *Nat. Rev. Immunol*. 9:581-593.

Thery, C., L. Zitvogel, and S. Amigorena. 2002. Exosomes: composition, biogenesis and function. *Nat. Rev. Immunol*. 2:569-579.

Van Damme, P., L. Martens, J. Van Damme, K. Hugelier, A. Staes, J. Vandekerckhove, and K. Gevaert. 2005. Caspase-specific and nonspecific in vivo protein processing during Fas-induced apoptosis. *Nat. Methods*. 2:771-777.

Wieman, H.L., S.R. Horn, S.R. Jacobs, B.J. Altman, S. Kornbluth, and J.C. Rathmell. 2009. An essential role for the Glut1 PDZ-binding motif in growth factor regulation of Glut1 degradation and trafficking. *Biochem. J*. 418:345-367.

Yannay-Cohen, N., I. Carmi-Levy, G. Kay, C.M. Yang, J.M. Han, D.M. Kemeny, S. Kim, H. Nechushtan, and E. Razin. 2009.

LysRS serves as a key signaling molecule in the immune response by regulating gene expression. *Mol. Cell.* 34:603-611.

국문초록

염증성 암세포에서의 caspase-8에 의존적인 lysyl tRNA syntetase의 exosome을 통한 분비 기전 연구

Lysyl-tRNA synthetase (KRS)은 본래 multi-tRNA synthetase(MSC)에 결합하여 단백질 합성에 관여하는 단백질로 알려져 있다. 또한 암세포 밖으로 분비 된 KRS는 대식세포로 인한 염증 반응을 유발 하는 것으로도 알려져 있다. 그러나 염증을 유발하는 KRS의 그 분비 기전에 대해서는 아직 알려져 있지 않다. 본 졸업논문에서는 KRS가 exosome을 통해서 암 세포로부터 분비되는 것으로 밝혔다. 세포 밖으로 분비되는 KRS는 exosome lumen 내에 위치하며, 대식세포 근처에서 exosome이 파열 되면서 exosome 밖으로 나와 대식세포를 자극하는것으로 나타났다. 기아 상태의 암세포에서 KRS의 N- 말단 12 아미노산 펩티드가 caspase-8에 의해 절단된다. N- 말단이 절단된 KRS는 KRS의 C- 말단에 있는 PDZ 결합 모티프를 노출시키게 된다. Syntenin은 KRS의 노출된 PDZ 결합 모티프와 결합하여 MSC와 결합되어 있는

KRS의 해리를 촉진 시켜서 exosome을 통한 분비가 이루어지게 한다. KRS를 가지고 있는 exosome은 대식세포의 이동과 TNF-α 분비를 유도하며 이 효과에 KRS는 크게 기여하고 있다. 본 졸업논문은 KRS를 통해서 aminoacyl tRNA synthetase의 분비 경로를 확립한 첫 논문이며, 암 세포에서 일어나는 caspase-8을 통한 염증반응에서 KRS의 잠재적 역할을 입증하였다.

주요어 : exosome, lysyl-trna synthetase, syntenin, caspase-8, inflammation

학번 : 2010-31385